ENERGY ABSORBING BEHAVIOUR OF GLASS FIBRE REINFORCED PVC TUBE UNDER QUASI-COMPRESSION

AHMAD RIDZUAN BIN SULAIMAN

UNIVERSITI TEKNIKAL MALAYSIA MELAKA

ENERGY ABSORBING BEHAVIOUR OF GLASS FIBRE REINFORCED PVC TUBE UNDER QUASI-COMPRESSION

AHMAD RIDZUAN BIN SULAIMAN

This report is submitted
in fulfillment of the requirement for the degree of
Bachelor of Mechanical Engineering

Faculty of Mechanical Engineering

UNIVERSITI TEKNIKAL MALAYSIA MELAKA

2022

DECLARATION

I declare that this project entitled "Energy Absorbing Behaviour of Glass Fibre Reinforced PVC Tube Under Quasi-Compression" is the result of my own work except as cited in the references.

Signature: .....

Name of student: Ahmad Ridzuan Bin Sulaiman

Date: .....

APPROVAL

I hereby declare that I have read this project report and in my opinion this report is sufficient in terms of scope and quality for the requirements of Bachelor Project.

Signature: ……

Name of lecturer: Prof. Madya Ir Dr. Sivakumar A/L Dhar Malingam

Date: ……

DEDICATION

Every difficult task necessitates our own efforts as well as the wisdom of seniors, particularly those who were dear to us in our upbringing. It is with great gratitude that I devote my little effort to my lovely and loving father and mother who's care, love, support, and pray throughout the day and night have enabled me to achieve such achievement and honour, as well as to all the hardworking and respected lecturers.

ABSTRACT

Throughout the years, the use of composite materials has increased significantly, owing to its good properties such as lightweight, excellent energy absorption capabilities, and excellent corrosion resistance. In this study, the polyvinyl chloride (PVC) tube with the glass fibre reinforced plastic (GFRP) as the reinforcement were tested to determine the crashworthiness parameter under quasi-compression test. There were four type of configuration for PVC/GFRP composites tube; PVC tube without fibreglass, with 0º/90º, -30º/60º and -45º/45º orientation of plain weave fibreglass. Thus, for each of the configuration type of composite tube, two different trigger mechanism were utilized that is composite tube without chamfer and with 45º internal single chamfer. The hand lay-up process was exploited for the fabrication of PVC/GFRP composite tube. From the finding, the reinforced PVC tube show better performance than the PVC tube alone. While, composites with 0º/90º oriented fibres parallel to the direction of compression had the highest specific energy absorption values, whereas PVC with no GFRP had the lowest specific energy absorption values. Thus, this study shows that by using trigger also can reduce the peak load value for all the specimen without drastically reducing the specific energy absorption value.

ABSTRAK

Sepanjang tahun, penggunaan bahan komposit telah meningkat dengan ketara, disebabkan sifatnya yang baik seperti ringan, keupayaan penyerapan tenaga yang sangat baik, dan rintangan kakisan yang sangat baik. Dalam kajian ini, tiub polivinil klorida (PVC) dengan plastik bertetulang gentian kaca (GFRP) sebagai tetulang telah diuji untuk menentukan parameter kebolehlanggaran di bawah ujian separa mampatan. Terdapat empat jenis konfigurasi untuk tiub komposit PVC/GFRP; Tiub PVC tanpa gentian kaca, dengan orientasi kaca gentian tenunan biasa 0º/90º, -30º/60º dan -45º/45º. Oleh itu, bagi setiap jenis konfigurasi tiub komposit, dua mekanisme pencetus yang berbeza telah digunakan iaitu tiub komposit tanpa chamfer dan dengan 45º internal single chamfer. Proses meletakkan tangan telah dieksploitasi untuk fabrikasi tiub komposit PVC/GFRP. Daripada penemuan, tiub PVC bertetulang menunjukkan prestasi yang lebih baik daripada tiub PVC sahaja. Manakala, komposit dengan gentian berorientasikan 0º/90º selari dengan arah mampatan mempunyai nilai penyerapan tenaga tentu yang tertinggi, manakala PVC tanpa GFRP mempunyai nilai penyerapan tenaga spesifik yang paling rendah. Oleh itu, kajian ini menunjukkan bahawa dengan menggunakan picu juga boleh mengurangkan nilai beban puncak bagi semua spesimen tanpa mengurangkan secara drastik nilai penyerapan tenaga spesifik.

ACKNOLEDGEMENT

IN THE NAME OF ALLAH
THE MOST GRACIOUS AND THE MOST MERCIFUL

Let me start by thanking my supervisor Prof. Madya Ir Dr. Sivakumar A/L Dhar Malingam from the Faculty of Mechanical Engineering at UTEM for his invaluable supervision, advice, guidance, encouragement, and support in completing this final year project report. He is a true inspiration to me as an engineering student.

At this point, I'd like to express my gratitude to Dr. Mohd Nur Azmi Bin Nordin from the Faculty of Mechanical Engineering for his guidance, suggestions, and evaluation of this project. This project would not have been possible without the financial assistance provided by the UTeM short-term grant funding.

A special thanks to the High Performance Structure laboratory technicians from the Faculty of Mechanical Engineering, Mr.Faizol Bin Kamarul Zahari and Mr. Faizal Bin Zailani, for their guidance, efforts and assistance in all lab and experiment works.

A special thanks to my family and friends for their continued encouragement and support throughout this final year of school and earning my bachelor's degree. Finally, I'd like to express my gratitude to everyone who was present during the most critical phases of this project's completion.

TABLE OF CONTENTS

LIST OF TABLES

LIST OF FIGURES

LIST OF ABBREVIATIONS

ECO	-	Economic Cooperation
CFRPs	-	Carbon fibre reinforced plastic composite
NC	-	No trigger/No chamfer
SC	-	45º internal single chamfer
PVC	-	Polyvinyl chloride
A	-	No fibreglass
B	-	Fibreglass with 0º/90º orientation
C	-	Fibreglass with -30º/60º orientation
D	-	Fibreglass with -45º/45º orientation
PVC/GFRP	-	PVC tube reinforced with GFRP
PMCs	-	Polymer matrix composites
MMCs	-	Metal matrix composites
CMCs	-	Ceramic matrix composites
NFCs	-	Natural fibre composites
PP	-	Polypropylene
PE	-	Polyethylene
UP	-	Unsaturated polyester
VE	-	Vinyl ester
GRP	-	Glass reinforced plastic
GFRP	-	Glass fibre reinforced polymer
GSRPCs	-	S-glass fibre reinforced polymer composites
IVI	-	Intermediate-velocity impact
SEA	-	Specific energy absorption
UD	-	Unidirectional
Pmena	-	Mean load
Pmax	-	Max load
CFE	-	Crush force efficiency

IPF	-	Initial peak force
EA	-	Energy absorption

CHAPTER 1

INTRODUCTION

1.1 Background

In recent years, vehicle manufacturers compete with one another in the automotive sector to make better vehicles that are of substantial quality in terms of performance and safety. Thus, the study of vehicle crashworthiness has become an important subject matter within the research domain, as automobile manufacturers attempt to build safer automobiles that are capable of preventing fatal injuries to passengers in the event of a collision. In order to determine crashworthiness, which is the study of plastic deformation of structures, tests have been conducted on a number of critical structures found on vehicles, including the frame of the vehicle, the subfloors of helicopters, and the highway barrier. The fundamental goal of doing such research is to ensure that individuals are protected in the case of tragic events such as impacts, crashes, and collisions occur (Abdullah et al.,2020)

There are a variety of products available to help drivers stay safe when they come to an abrupt stop or accident. These products include bumpers, seat belts, airbags, and anti-lock braking systems (ABS). Aside from safety, pollution is a significant and critical issue. The automobiles emit large amounts of toxic gases such as Nitrogen Dioxide (NO2) and Carbon Dioxide (CO2), which were a significant contributor to global warming. Vehicles for economic cooperation (ECO) are becoming increasingly popular as a result of the pressing need to conserve energy while also safeguarding the environment. It is an effective method of increasing fuel efficiency by lowering the weight of automobiles on the road. Traditional metal materials, on the other hand, have a difficult time achieving strong energy absorption qualities while remaining lightweight. As a result, it was suggested that novel material

systems may be used to replace traditional metal materials in the production of next-generation cars. Particularly in this field, fibre reinforced composites (CFRPs) have gained a lot of attention (Ma et al.,2015)

In addition, CFRP feature high stiffness to weight and strength to weight ratios, as well as outstanding fatigue and corrosion resistance, which makes them ideal for aerospace applications. They are extremely desirable as materials for crashworthiness applications because of their combination of characteristics. Composite materials that are reinforced with glass fibres account for an important share of composite applications. For one thing, composites containing additional types of reinforcing materials, such as carbon and aramid fibres, are significantly more expensive than those having only glass fibres. GFRP composites have a higher rigidity than aluminium and a specific gravity that is one-quarter that of steel when the composition and fibre orientation are appropriate (Khan et al.,2015). GFRPs have been employed in a variety of industries, including automotive applications, aerospace applications, civil infrastructures, marine applications, and the pipe industry. While employing composites for crashworthiness, the issue is to use precise geometry and materials to permit higher safety standards while keeping weight as low as possible. This should be accomplished while not surpassing what would be deemed acceptable production costs in the industry (Khan et al.,2021).

1.2 Problem Statement

The weight of a vehicle accounts for approximately 75% of the total gasoline utilised by the vehicle (Khan et al.,2021). On the basis of current estimates, it should be able to reduce a vehicle's weight by approximately 10% while simultaneously reducing its fuel consumption by up to 8%. This reduction translates into a large reduction in the amount of carbon dioxide emitted by a vehicle over the course of its operational life. By using GFRP composites, the weight can be reduced while maintaining the crashworthiness properties

parameter. Thus, experiment need to be conduct to find the properties of energy absorption and crashworthiness parameter under quasi-loading.

1.3 Objectives

The objectives of the project are:

1. To study the effect of different trigger mechanism.
2. To study the effect of different degree orientation for plain weave fibreglass.

1.4 Scope of Project

Scope of this project are:

1. Produce two type of trigger geometry, no trigger (NC) and 45º internal single chamfer (SC)
2. Produce PVC pipe with four different plain weave fibreglass orientation, (A) no fibreglass, (B) 0º/90º, (C) -30º/60º and (D)-45º/45º,
3. To conduct the quasi-static compression test.
4. To analysed the mechanical properties and crashworthiness parameter for each of the specimen tested.

1.5 General Methodology

The strategy begins with the objective and the problem statement as a first step. After the purpose already defined, it needs to do some literature review to gain more knowledge or facts about this project. Then fabricating the specimen to with two different trigger mechanism with different degree orientation lay-up of plain weave fibreglass. Test the specimen by using quasi static loading to get the desired data for the energy absorption and crashworthiness parameter.

After the researcher gets the data that shows the mechanical properties of each of the PVC/GFRP tube composites, the analysis will be done by calculation and graph from the

data collect during the experiment to obtain the final result of the experiment. Finally, after all step have completed, the researcher can make a conclusion. Figure 1.1 show the general flowchart.

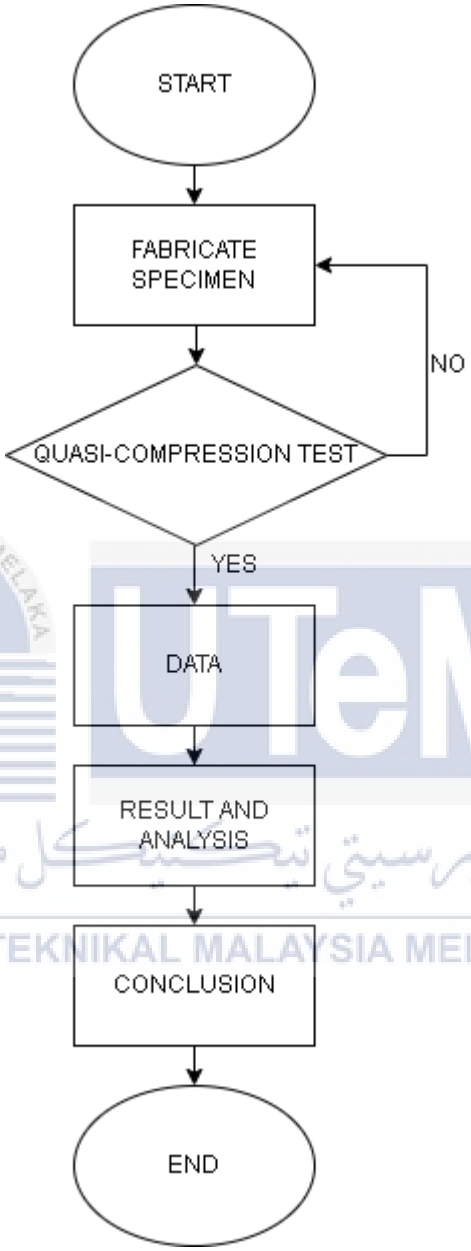

Figure 1.1: General Flowchart

CHAPTER 2

LITERATURE REVIEW

2.1 Introduction

This chapter will broaden the understanding and compare the assessment of various researchers for tube composites fibre based on its constituents, manufacture method, mechanical properties and failure by using compression test. On top of that, this chapter also provide the potential results of the research and present comprehension of the subject.

2.2 Composites

A composites material is made up by combining two or more chemically or physical dissimilar material that have a discrete interface. The elemental materials retain their individual identity in the composite at least microscopically, although they have different qualities and characteristics than the elements, their combination produces attributes that are diverse from those of constituents**.** The matrix is one of these constituents that forms a continuous phase. The other major component is a reinforcement in the form of fibres or particulates that is added to the matrix in order to improve or change its properties. The reinforcement is dispersed uniformly throughout the matrix in a discontinuous phase. The reinforcement surface may be chemically treated or coated with a very thin layer of polymer to facilitate wetting of the reinforcement by the matrix, as well as control or enhance interfacial bonding between the reinforcement and the matrix. It is also possible that the surface treatment will protect the reinforcing surface from deterioration caused by external attack, such as moisture and chemicals, or by an undesirable chemical reaction with the matrix when exposed to high temperatures (Mallick,1997).

Besides, a composite's matrix material can be a polymer (PMC), metal (MMC), or ceramic (CMC). Composite materials are classified as PMCs, MMCs, or CMCs depending on matrix apply. The majority of commercially available composites are made of polymer matrices; however, MMCs and CMCs are gaining high demand in high-temperature applications. Figure 2.1 show how the composite can be formed.

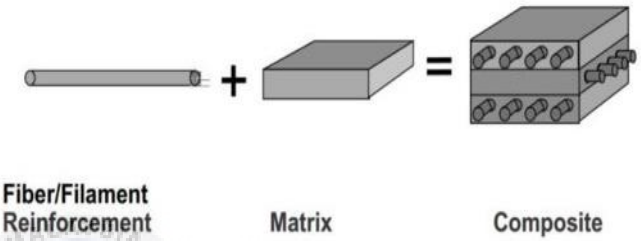

Figure 2.1: composites ((Kumar and Lohchab, 2016)

2.3 Matrix

The processing characteristics are heavily influenced by the matrix used. The time needed to complete the chemical or curing reaction that alter the liquid thermosetting polymer into a solid polymer, for example, determines the moulding time of a thermosetting polymer matrix composite. Besides, the chemistry and stoichiometry of the reactants, which include the prepolymer and the curing agent, determine the curing time. The viscosity of the thermosetting polymer is also significant, as it influences the polymer's flow characteristics in the mould. This, in turn, affects the matrix's wetting of fibres, as well as the void content in the matrix (Mallick,1997). Table 2.1 show the type of matrix that commonly used nowadays.

Table 2.1: Matrix Materials Commonly Used in Advanced Composite

(Mallick,1997)

Polymeric
Thermoset resins
Epoxies: Principally used in aerospace, aircraft, and sporting goods applications
Polyesters and vinyl esters: Principally used in automotive, marine, chemical, electrical, and consumer goods applications
Polyurethanes and polyurea: Principally used in reaction injection molding process for manufacturing automotive body parts
Phenolics: Used in both aerospace and automotive applications
Bismaleimides, polyimides, polybenzimidazoles, etc.: Used for high-temperature aerospace applications
Thermoplastics
Nylon 6,6, Nylon 6, thermoplastic polyesters (such as PET and PBT), polycarbonate, polyacetals, polypropylene, etc.: Used with discontinuous fibers in injection molded articles
Polyether ether ketone (PEEK), polyphenylene sulfide (PPS), polysulfone (PSUL), polyamide-imide (PAI), polyether imide (PEI), etc.: Used with both continuous and discontinuous fibers for moderately high-temperature applications
Metallic
Aluminum alloys, titanium alloys, magnesium alloys, copper-based alloys, nickel-based alloys: Used for moderately high-temperature applications
Ceramic
Silicon carbide (SiC), aluminum oxide (Al_2O_3), silicon nitride (Si_3N_4), carbon: Used for high-temperature applications

Polymeric matrices are currently the most commonly used in natural fibre composites (NFCs) because they are light weight and can be processed at low temperatures. For natural fibre matrices, both thermoplastic and thermoset polymers have been used. Most natural fibres used for reinforcement in natural fibre composites are thermally unstable above 200 ºC, though they can be processed at higher temperatures for a short time under certain conditions. Indeed, the thermoplastic matrices PP and PE are the most commonly used for NFCs. Unsaturated polyester (UP), epoxy resin, phenol formaldehyde, and VE resins are the most commonly used thermosets. Thermoplastics can be repeatedly softened and hardened by heating and cooling, and they have the potential to be the most easily recycled materials (Pickering et al.,2016).

2.4 Synthetic Fibres

Synthetic fibres are form by polymers that do not occur naturally and are made entirely in the lab, usually from petroleum by products. Synthetic fibres are made from a variety of chemicals, each with its own set of characteristics. Nylon, polyesters, acrylics, polyurethanes, and other polymers are used to make fibre. Synthetic fibres have a longer length and are more durable. In Figure 2.2, Kevlar (aramid), carbon, and glass fibres are the three most common synthetic fibres used in composites (Saba and Jawaid,2017).

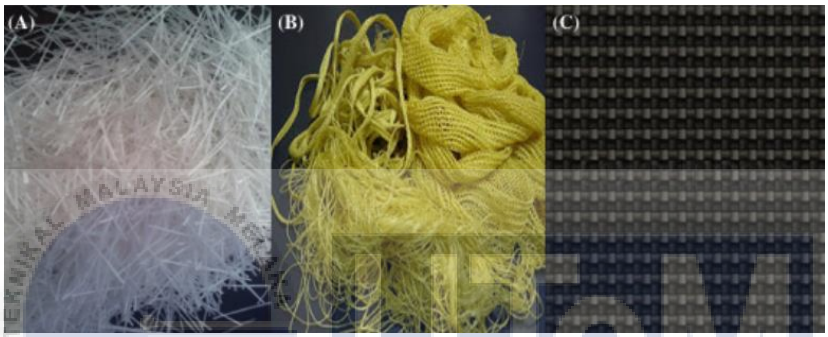

Figure 2.2: A(glassfibre), B(Kevlar) and C(Carbon). (Saba and Jawaid,2017)

Synthetic fibres are more durable than natural fibres and will take on a variety of colours quickly. Furthermore, many synthetic fibres provide benefits to consumers such as stretching, waterproofing, and stain resistance. All fibres break down and erode as a result of sunlight, dampness, and human skin oils. Hence, mechanical strength of synthetic fibre-based materials is far superior to that of natural fibre-based composites (Chandrasekar et al.,2018). Figure 2.3 show the type of fibre class and subclassification.

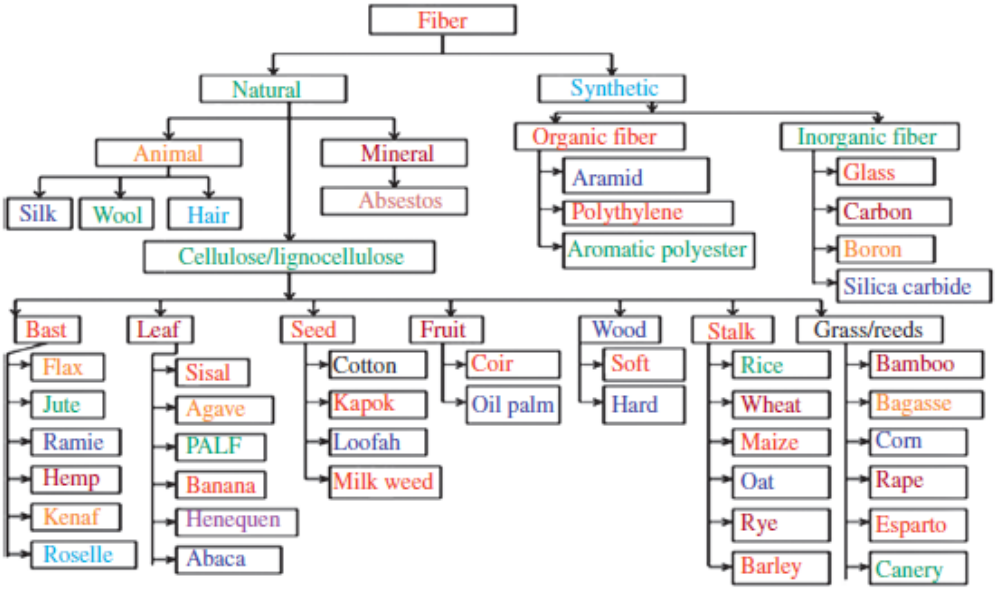

Figure 2.3: Class and subclassification of fibre. (Saba and Jawaid,2017)

2.4.1 Glass Fibre

Glass fibres (GF), which have a high percentage (50%) of silica content, as well as diverse mineral oxides, are the most versatile and inexpensive synthetic fibres compared to Kevlar and carbon, and are widely utilised in the polymer composites industries (Saba and Jawaid,2017). GF is made up of very fine glass fibres. Extrusion of very thin strands of silica-based or other formulation glass is used to create it. When compared to carbon fibre or other plastic fibres, glass fibre is substantially less expensive and less fragile. It can be used as a reinforcing ingredient to boost the strength and reduce the weight of numerous polymer composites. Glass reinforced plastic (GRP), commonly known as 'fibreglass,' is one such material. E-glass, an alumina-borosilicate glass used mostly in glass reinforced plastics, is the most common glass fibre utilised. A-glass, E-CR-glass, C-glass, D-glass, R-glass, and S-glass are some of the other varieties of glass used (Batabyal et al., 2018). Figure 2.4 shows

the general view of composites uses for aeroplane and Table 2.2 show the comparison between glass fibre and natural fibre.

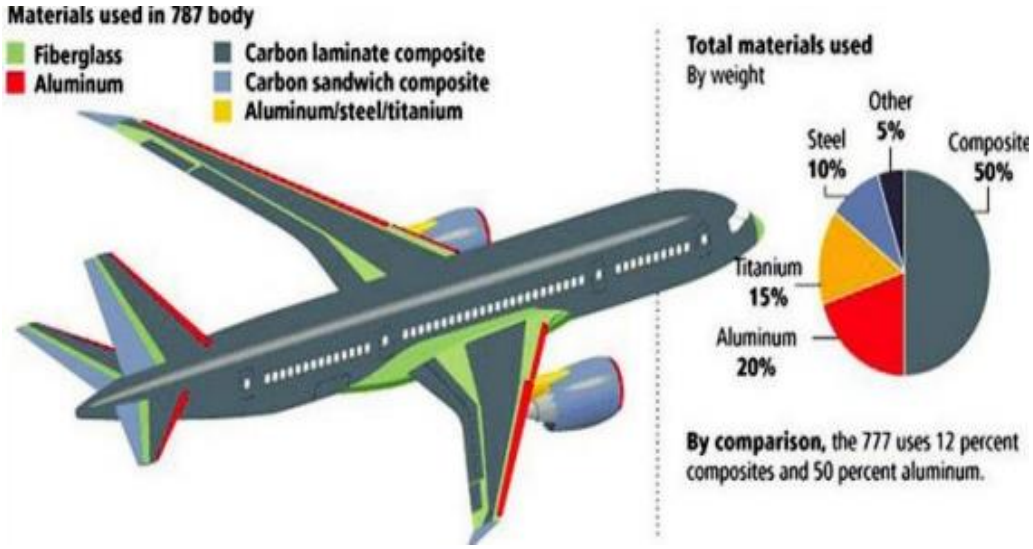

Figure:2.4 Material used in Boeing787 (Batabyal et al., 2018)

Table 2.2: Comparison between glass fibre and natural fibre (Wambua et al,.2003)

Component	Glass fibre	Natural fibre
Density	Twice than natural fibres	Low
Cost	Low (Higher than natural fibre)	Low
Renewability	No	Yes
Recyclability	No	Yes
Energy consumption	High	Low
Distribution	Wide	Wide
CO_2 neutral	No	Yes
Abrasion to machines	Yes	No
Health risk when inhaled	Yes	No
Disposal	Not biodegradable	Biodegradable

2.4.2 Properties of Glass Fibre

Glass fibre had been used widely due to the high mechanical properties. GF are a material that is lightweight, less brittle, less stiff, exceptionally strong, and durable (Saba and Jawaid,2017). Fibreglass is extremely resistant to both tensile and compressive stresses. Thermal insulation, electrical insulation, sound insulation, corrosion-resistant fabrics, high strength fabrics, and more applications use glass fibres. They're commonly employed in the construction of FRP tanks and vessels (Batabyal et al.,2018). Table 2.3 show the mechanical and thermal properties of the glass fibre.

Table 2.3: Mechanical and thermal properties of various types of glass fibre (Sathishkumar et al.,2018)

Fibre	Density (g/cm3)	Tensile strength (GPa)	Young's modulus (GPa)	Elongation (%)	Coefficient of thermal expansion (10^{-7}/°C)	Poison's ratio	Refractive index
E-glass	2.58	3.445	72.3	4.8	54	0.2	1.558
C-glass	2.52	3.310	68.9	4.8	63	-	1.553
S2-glass	2.46	4.890	86.9	5.7	16	0.22	1.521
A-glass	2.44	3.310	68.9	4.8	73	-	1.538
D-glass	2.11-2.14	2.415	51.7	4.6	25	-	1.465
R-glass	2.54	4.135	85.5	4.8	33	-	1.546
EGR-glass	2.72	3.445	80.3	4.8	59	-	1.579
AR glass	2.70	3.241	73.1	4.4	65	-	1.562

2.4.3 Glass Fibre Reinforced Polymer (GFRP)

Composite materials were most often made up of glass fibre-reinforced polymeric (GFRP) composites. Organic, polyester, thermostable, vinyl ester, phenolic, and epoxy resins were used in the matrix. The required physical and functional features of GFRP composites were equal to steel, had better stiffness than aluminium, and the specific gravity was one-quarter that of steel due to appropriate fibre compositions and orientation. The mechanical behaviour of a fibre-reinforced composite is mostly determined by fibre strength and modulus, chemical stability, matrix strength, and stress transmission interface bonding between fibre and matrix (Batabyal et al.,2018).

Besides, S-glass has a higher modulus and tensile strength than E-glass. However, due to its lower cost, E-glass fibre is more popular than S-glass. A minor quantity of zirconium is present in alkali-resistant glass fibres, which helps to avoid corrosion caused by alkali contact. GSRPCs are now often found in electronic components such as circuit boards, televisions, radios, computers, and phones. These composites are also used in a variety of other applications, including housewares, construction, aerospace, boats, marine, and medical applications (Gupta, 2018). In the Table 2.4, the mechanical and thermal properties of woven GFRP is stated.

Table 2.4: mechanical and thermal properties of GFRP (Işık and Ekici, 2010)

Specific weight	2.03 g/cm^2
Fibre diameter	22 µm
Flexural strength (DIN EN 63)	98 N/mm^2
Tensile modulus (DIN 53457	3450 N/mm^2
Tensile strength (DIN EN 61)	48 N/mm^2

Tensile elongation (DIN EN 61)	5 %
Cure contraction (DIN 16946)	65 %
Temperature of deflection (DIN 53461)	70 ℃
Martens temperature (DIN 53458)	50 ℃
Thermal conductivity (DIN 52612)	0.15 W/m℃
Heat specific	1.46 kj/kg℃

2.5 Fabrication Method

2.5.1 Hand Lay Up

When it comes to polymer composite product development, the hand lay-up technique is most commonly associated with open moulding processing. It takes a highly skilled operator to perform the fabrication operation with precision and accuracy. A mould release agent is necessary before fabrication in order to facilitate the handling of composites and generate a smooth surface on the finished piece of work. Before combining the fibre and matrix, it is necessary to calculate the density of the resulting composite; this will allow you to use the least quantity of raw material possible. The technique can be used with small-sized fibres, fibre mats, and fabrics. Various thermosets and thermoplastics, including UPE, polyurethane, phenolic, vinyl ester, polylactic acid (PLA), and epoxy, are appropriate for hand lay-up processes. A hand lay-up is sometimes referred to as a wet lay-up in some circles. When using natural fibre composites for automotive components, automobile manufacturers rely on the hand lay-up approach (Asim et al.,2017.)

The hand lay-up process is the most ancient way of woven composite manufacture still in use today. The samples are prepared in accordance with a set of guidelines. First and foremost, the mould surface is coated with a release anti-adhesive chemical in order to prevent polymer from adhering to the surface. Afterwards, a thin plastic layer is put to both the top and bottom of the mould plate in order to provide a smooth finish on the final product. It is necessary to cut the layers of woven reinforcement into the required shapes and position them on the mould surface. As previously said, the resin is blended with other materials and infused onto the surface of reinforcement that has already been placed in the mould with the aid of a brush to ensure that it is evenly distributed. After that, the additional mats are placed on top of the previous polymer layer and pressed down with a roller to eliminate any trapped air bubbles as well as any extra polymer that may have formed. After then, the mould is closed and the pressure is released, resulting in a single mat. The mould is opened and the woven composite is removed from the mould surface after it has been allowed to cure at room temperature. The schematic of hand lay-up is shown in Figure 2.5 (Raji et al.,2019)

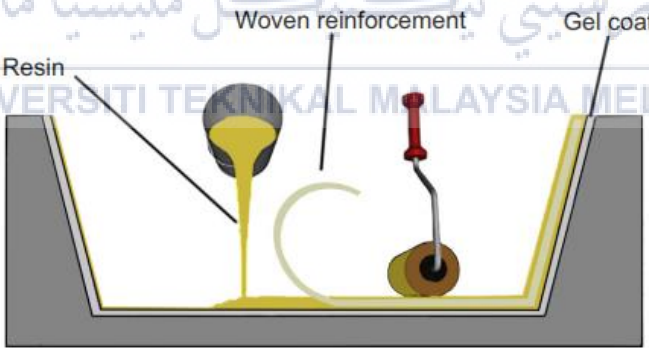

Figure 2.5: Hand lay-up process. (Raji et al.,2019)

2.6 Factor That Affect Energy Absorption.

2.6.1 Fibre Orientation

From the previous study conducted by Supian et al., (2021) on (Effect of winding orientation on energy absorption and failure modes of filament wound kenaf/glass fibre reinforced epoxy hybrid composite tubes under intermediate-velocity impact (IVI) load). After being subjected to axial intermediate velocity impact loading, the behaviour and strength of hybrid kenaf/glass fibre-reinforced epoxy tubes were investigated experimentally. The specimens subjected to axial intermediate-velocity impact have three filament winding orientation parameters of 30º, 45º, and 70º of hybrid kenaf/glass fibre-reinforced epoxy and glass fibre reinforced-epoxy, respectively. To produce a good intraply hybrid kenaf/glass composite tube fabrication technique, all materials and samples were fabricated at the SIRIM STV Malaysia laboratory using an automated filament winding machine. The study's findings revealed that the concept of constructing intraply hybrid filament winding technology of natural/synthetic materials performed similarly to the physical crashworthiness of synthetic composite tube with distinct progressive crushing behaviours. Also revealed was that winding orientation parameters at 30°, 45°, and 70° of the hybrid composite tube increased the energy absorber capabilities by 33 %, 34 %, and 56 %, as compared to the glass fibre reinforced polymer (GFRP).

In the study from Zhang et al., (2018). The influence of axil layups and fibre orientation of E-glass/ PET199 tubes to total energy absorption was investigated under a variety of various stress circumstances. The orientation of the fibres in the winding process of creating composite tubes was optimised. To ensure that the optimal results were achieved, quasi-static compression tests and drop weight tests were carried out. According to the

findings of this investigation, the best layup condition is [65/10/65/10/65]. Too much axial layup reduces a tube's specific energy absorption, implying that ply orientation has a substantial impact on the energy absorption of composite tubes. The SEA of GFRP tubes achieved by dynamic impact tests was approximately 10% lower than that obtained during quasi-static compression tests. The impact speed of 3–5 m/s resulted in a decrease in SEA and a strong serration of the load-displacement curve. Based on the numerical modelling and experimental results, it is discovered that improving layup condition and layup orientation can improve the energy absorption capacity of GFRP tubes.

From the previous study by Chambe et al., (2019), in order to analyse and compare the ability of various composite constructions to disperse the energy generated following a collision .Circular composite tubes were examined under compression to identify their behaviour and determine their absorbing capabilities, which were determined using the specific energy absorption method (energy absorbed per unit weight). The study examined a number of different composite tubular structures made of various materials and architectural configurations, including a hybrid composition of carbon fibre and aramid fibre, as well as hybrid configurations of 0º/90º UD with either woven or braided fabric. Multiple innovative and experimental trigger systems have been examined in order to see if they may improve the absorption capabilities of the structures under consideration. Specimens with 0º oriented fibres coinciding with the direction of compression had the highest specific energy absorption values, whereas specimens with no fibre oriented in this direction had the lowest specific energy absorption values.

2.6.2 Trigger Mechanism.

Based on the finding by Sivagurunathan et al., (2018). It was discovered that by selecting a suitable trigger mechanism while maintaining crashworthiness optimization, the energy absorption performance of jute/epoxy composite tubes may be improved. The tulip

trigger mechanism considered to be favourable as it recorded the highest Pmean, energy absorption, specific energy absorption, and crush force efficiency values compared to other trigger mechanisms. Nevertheless, the total number of triggered tubes did not result in a decrease in peak load as compared to the total number of non-triggered tubes, but it did result a considerable gain in energy absorption capacity, mean load, and crush force efficiency. Furthermore, the use of triggering mechanisms resulted in a considerable increase in the CFE values over time. Also, with the exception of the non-triggered tubes, the majority of the triggered tubes showed gradual failure. On the whole, the tulip trigger structure was acknowledged with the greatest amount of energy absorption.

Nasir Hussain et al., (2020). conclude that when notch triggers for square, cylindrical, and hexagonal shapes were used in conjunction with GFRP crash boxes, it was noted that the crashworthiness of the GFRP crash boxes was significantly improved. However, the decagonal crash box revealed an unusual behaviour in which the SEA was highest for cases where there was no trigger. Because composite parts exhibit complex behaviour when subjected to impact loading, it is critical to understand the influence of changes in geometrical shapes and features. This understanding will aid in the improvement of the crashworthiness behaviour of parts constructed of composite materials. It can be deduced that a particular form of trigger that increases the crashworthiness of a given geometrical shape may not be effective for other sorts of geometrical shapes of the same or different types. In order to effectively use triggers, it is necessary to understand the behaviour of each geometric shape, as well as the various patterns of triggers, because the trigger that is most effective for one type of geometry may be the worst for another type of geometry.

2.7 Quasi-Compression

2.7.1 Crushing Speed and Range

From the previous study for the PVC/GFRP composite, Khan et al.,(2021), The INSTRON material testing machine was used to perform a quasi-static crushing test on the samples .Before each test began, the upper and lower plates were adjusted so that they would make contact with the upper and bottom surfaces of the tested specimen, respectively. As part of the crushing test, the lower plate of the testing machine was left static/stationary, while the upper plate moved downwards at a steady speed. All specimens with height 100mm and inner diameter 50mm were crushed at a rate of 500 mm/min, up to a displacement of 75 mm, until they were completely crushed. The PVC specimens, on the other hand, were an exception, as they experienced material densification at displacements greater than 75 mm.

Albahash and Ansari,(2017), utilized the crushing test for the natural and hybrid fibre Crushing tests were performed on the specimens using a computer-controlled servo-hydraulic INSTRON machine, system ID (4469 H2005), with a scale load of 100 kN and a speed of 15 mm/s using a computer-controlled servo-hydraulic INSTRON machine. The specimens were all crushed at a crushing distance of 80 mm between each other. During the crushing test for each specimen, images were captured at various phases of the crushing process in order to demonstrate the many failure modes that might occur.

Sivagurunathan et al., (2018b) conducted a study about the square tube utilizing the axial-quasi static crushing test. A series of axial quasi-static crushing tests were carried out using a conventional testing machine at a constant crosshead displacement rate, with the results being reported. Testing was conducted out at the Universiti Teknikal Malaysia Melaka (UTeM) in Malaysia on a Shimadzu AG-I Universal Testing Machine equipped with

a 100 kN load cell, with a constant crosshead speed of 10 mm/minute for each specimen under consideration. The test was performed in accordance with the ASTM-D3410 standard, with the stroke length set at 90 mm. Axial crushing was achieved by placing all of the specimens on the bottom platen and crushing them between two parallel steel flat platens.

The data was then transferred from the testing machine to a computer and stored on a hard drive. The whole set of quasi-static tests was carried out beyond the initial point of densification of the specimens or until the bottoming-out displacement for tube materials was reached, whichever came first. Throughout the entire compression test, the mechanisms of failure were examined and images of the deformation process were taken for the purpose of analysis. Energy absorption and crashworthiness properties of the materials were determined based on the load–displacement data collected.

CHAPTER 3

METHODOLOGY

3.1 Introduction

This chapter describes the philosophical aspect of this investigation, which is based on data gathered from previous studies. This chapter will focus at the fabrication and testing procedures for PVC reinforced GFRP, such as composite preparation, PVC/GFRP tube composite method fabrication, trigger mechanism and specimen arrangement for compression test. Figure 3.1 show the flowchart of the project.

3.2 Tube Composite Fabrication Process

Figure 3.1, the all process of the fabrication of PVC/GFRP composite tube is shown in the flowchart. There is two tube that doesn't have fibre glass and the other six reinforced GFRP with different degree of orientation, a) 0º/90º b)-45º/45º and c)-60º/30º. Two different geometry is applied to the specimen a) No Trigger (NC) and b) 45ºInternal Single Chamfered Trigger (SC) for each type degree of orientation for fibreglass.

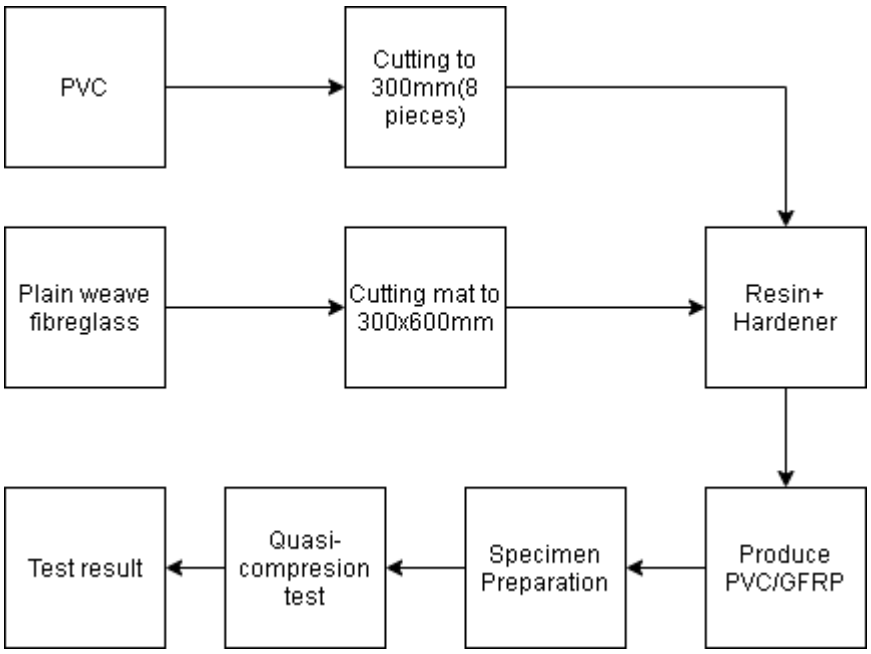

Figure 3.1: PVC reinforced GFRP composites fabrication process flowchart.

3.3 PVC/GFRP Composite Fabrication

In this study, the plain weave fibre glass (purchased from MC Fibreglass, Malaysia) was use as the synthetic fibre to reinforced the PVC tube (purchased from KimHai Hardware Sdn. Bhd.) that have inner diameter of 53mm with thickness 7mm. The unsaturated epoxy resin(P9509/NW) with density of 1.3 g/cm^3 and MEPOX MEKP catalyst as the hardener (purchase from LEZO, Malaysia) serving as the matrix. Figure 3.2 shows the plain weave fibre glass and Figure 3.3 show the epoxy resin with hardener. Table 3.1 show the mechanical properties of the epoxy resin, fibreglass and PVC

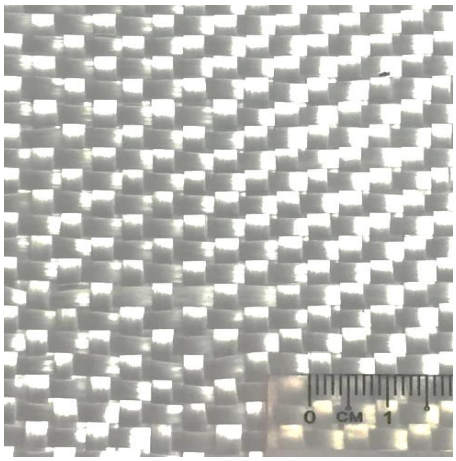

Figure 3.2: Plain weave fibreglass

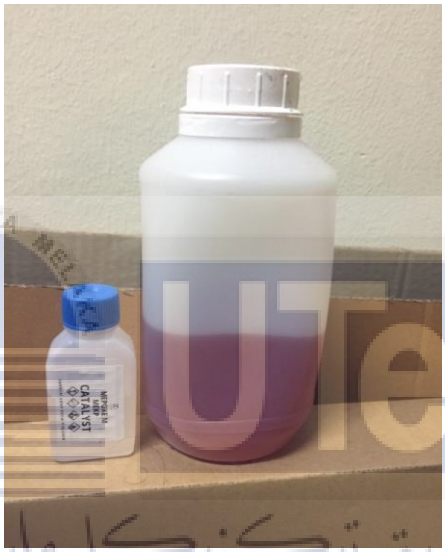

Figure 3.3: Epoxy resin and hardener

Table 3.1: Mechanical properties for the epoxy resin, fibreglass and PVC (Khan et al.,2021)

Properties	Epoxy Resin	Fibreglass	PVC
Tensile strength (MPa)	33.5-70	2000-3500	40.69
Tensile Modulus (GPa)	3.102-10.6	70-76	1.00
Strain at break (%)	-	1.8-4.8	-
Density (g/cm^3	1.3-2	2.5	-

The PVC tube were cut to prepare 8 samples with length approximate 300mm (show in Figure 3.4) each. To form the PVC/GFRP composite tube with 3 layer of plain weave fibreglass., the plain weave fibreglass mat is cut to form rectangular shape with dimension 300mm x 600mm (Figure 3.5) according to the desire orientation degree desire that is (0º/90º) , (-30º/60º) and (-45º/45º) as shown in Figure 3.6: (A),(B) and (C).

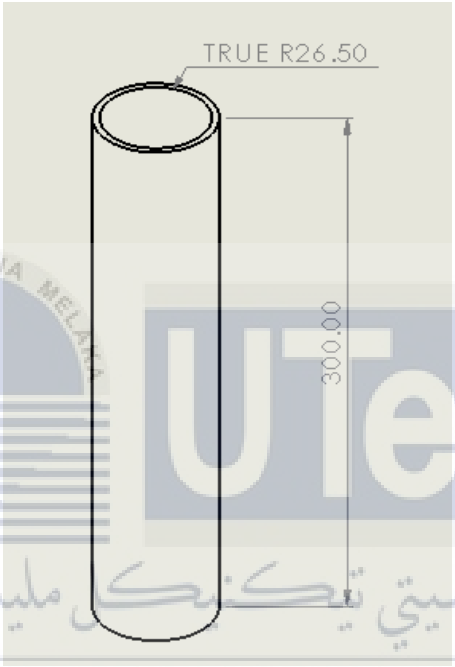

Figure 3.4: PVC tube

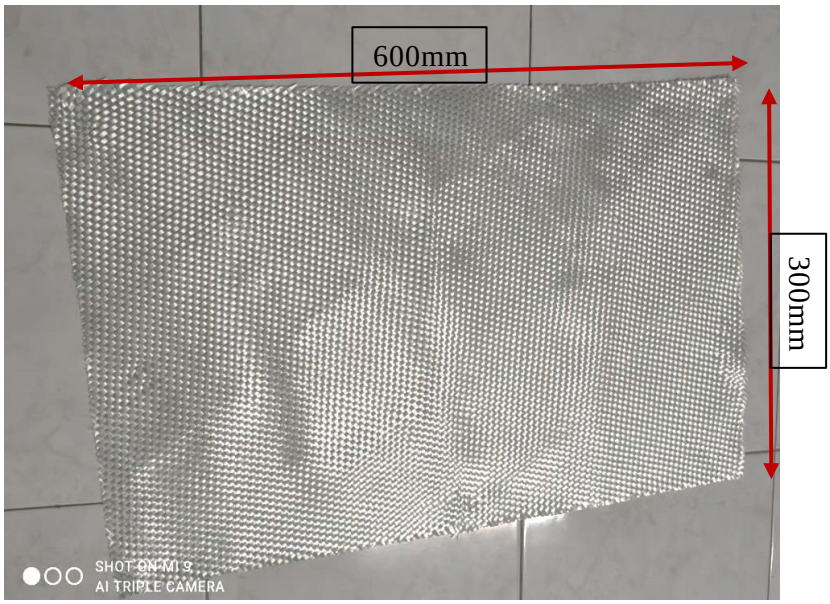

Figure 3.5: Rectangular plain weave fibreglass mat

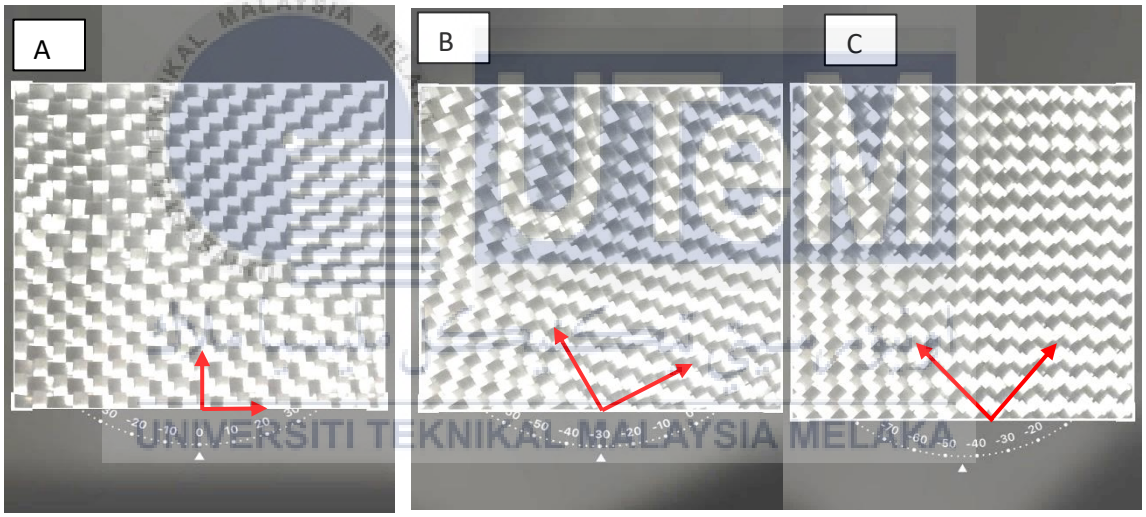

Figure 3.6: Degree orientation of the fibreglass., A(0º/90º), B(-30º/60º), C(-45º/45º)

In this fabrication proses, hand layup method was utilized. Before wrapping the PVC tube with the fibreglass, the PVC tube outer surface need to be roughed by using sand paper to make sure the surface contact between PVC and GFRP is strong thus make the GFRP strongly stick to the PVC tube surface. After the roughing process for the 6 samples tube. The preparation for wrapping is done by mixing the epoxy resin and hardener with ratio 100:1 by measured using measuring scale shown in Figure 3.7. After that, the wetting process is done by pouring the epoxy on the rectangular mat and spread the epoxy by using

brush as shown in Figure 3.8 until the fibreglass mat completely wet. Then the wrapping process is done by slowly rolling the PVC tube with the wet fibreglass rectangular mat shown in Figure 3.9 to form the PVC/GFRP composite in Figure 3.10. For the curing process, the PVC/GFRP composites was dried at room temperature for 2 hours. The PVC/GFRP composite completely dry after 4 hours. For better curing effect, the PVC/GFRP composite dry for 24 hours at room temperature.

Figure 3.7: Measuring scale

Figure 3.8: Wetting the fibreglass mat

Figure 3.9: Wrapping process

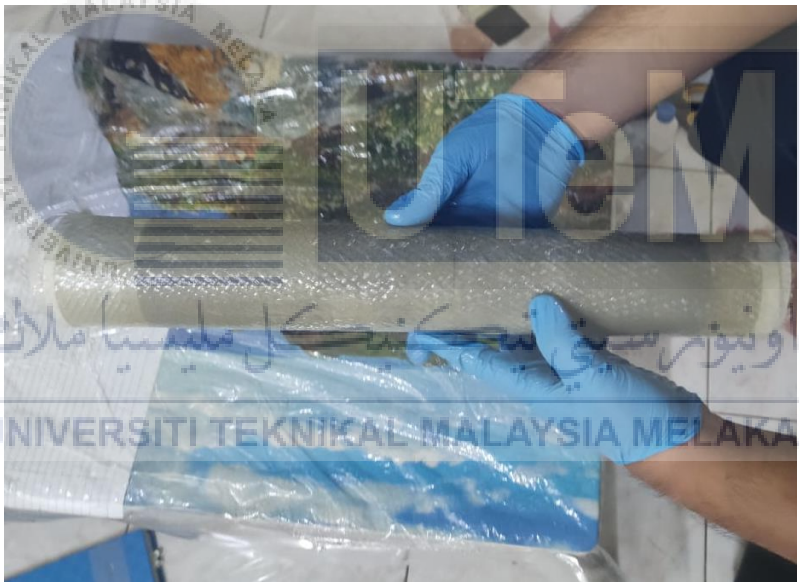

Figure 3.10: PVC/GFRP composite tube

3.4 Specimen Preparation

The tube specimen will have the length 100mm, in this study, no trigger (NC) and 45º internal single chamfer (SC) were applied. Table 3.2 shows the sample for composite tube with length 300mm.

Table 3.2: Composite tube with 300mm length

Type.	Fibreglass Orientation (º)	No of sample	Type of composite
A	No fibreglass	2	PVC
B	0º/90º	2	PVC/GFRP
C	-30º/60º	2	PVC/GFRP
D	-45º/45º	2	PVC/GFRP

3.4.1 No Trigger Preparation

For the no trigger (NC) configuration, select 1 tube from each type of composite tube A, B, C and D and cutting the 300mm composite tube to form 3 composite tube that have 100mm length. Then flatten and smoothen the cutting surface of every specimen by utilized the lathe machine to get the best surface contact. The Figure 3.11 show the no trigger geometry and Table 3.3 show the code for NC.

Figure 3.11: No trigger composite tube

Table 3.3: Code for NC

Code.	Fibreglass Orientation (º)	No of sample	Type of composite
ANC	No fibreglass	3	PVC
BNC	0º/90º	3	PVC/GFRP
CNC	-30º/60º	3	PVC/GFRP
DNC	-45º/45º	3	PVC/GFRP

3.4.2 45º Internal Single Chamfer Trigger

For the 45º internal single chamfer (SC) specimen, the 300mm length tube were cut to form 3 tube that have 100mm length each for every type of the specimen. Then, the lathe machine in Figure 3.12 was used to construct the internal single chamfered (show in Figure 3.13) and flatten and smoothen the cutting surface each of the specimen. Figure 3.14 show the cutting process for the internal single chamfer (SC) and Table 3.4 shows code for SC.

Figure 3.12: Lathe Machine

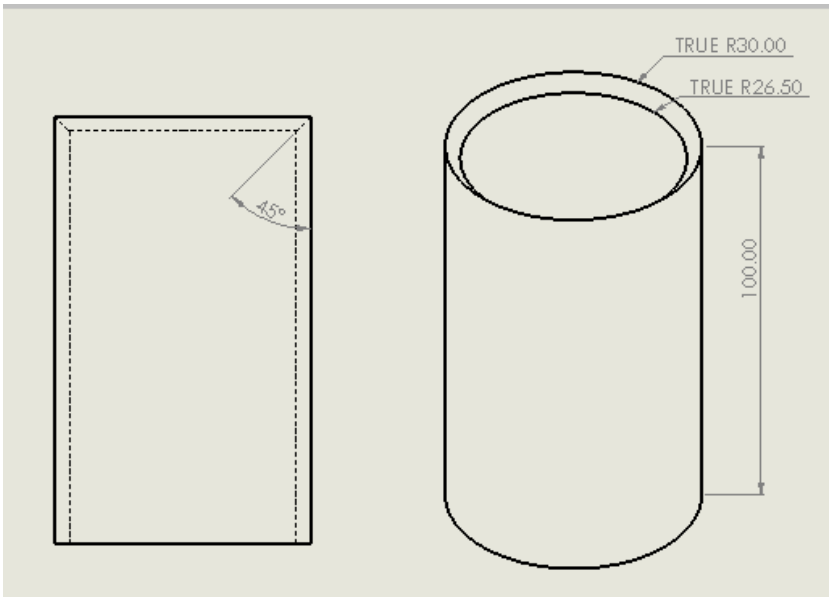

Figure 3.13:45º internal single chamfer trigger composite tube

Figure 3.14: Cutting process for SC

Table 3.4: Code for SC

Code.	Fibreglass Orientation (º)	No of sample	Type of composite
ASC	No fibreglass	3	PVC
BSC	0º/90º	3	PVC/GFRP
CSC	-30º/60º	3	PVC/GFRP
DSC	-45º/45º	3	PVC/GFRP

3.4.3 Labelling and Weighing the Specimen

The last procedure is to label and weight each of the specimen. Table 3.5 shows the mass of every specimen and the Figure 3.15 show the specimen that have been labelled.

Table 3.5: Mass of the specimens.

Type	Mass(g)	Type	Mass(g)	Type	Mass(g)	Type	Mass(g)
ANC1	91	BNC1	140	CNC1	154	DNC1	147
ANC2	93	BNC2	140	CNC2	148	DNC2	149
ANC3	91	BNC3	139	CNC3	154	DNC3	149
ASC1	89	BSC1	141	CSC1	148	DSC1	150
ASC2	91	BSC2	141	CSC2	144	DSC2	150
ASC3	92	BSC3	142	CSC3	147	DSC3	151

Figure 3.15: Labelled specimen

3.5 Quasi-Compression Testing

For compression test, the INSTRON 5585 Universal Testing Machine (UTM) with load cell 150kN (shown in Figure 3.16) was utilized to get the raw data for crashworthiness parameter. The most crucial data needed is the load - displacement. From the data obtain, the peak load (Pmax), mean load (Pmean), energy absorption (EA), specific energy absorption (SEA) and crush force efficiency (CFE) can be obtain directly from the data and from calculation from the data obtained.

Figure 3.16: INSTRON 5585 Universal Testing Machine (UTM)

To obtain results from compression test at UTM machine, Bluehill software is used. The parameter for testing is being kept constant for all specimens. Table 3.6 shows the parameter used.

Table 3.6 Parameter for compression test

Parameter	Value
Crosshead Speed Rate	500mm/min
Displacement	80mm

The tube composite specimen is placed at the middle of compression jig and the level of the jig is adjusted close to the specimen until approximately as close as a piece of paper for the gap between the specimen and the upper jig. The levelling of the jig is adjusted by pushing the jog down or jog up button on the side of Instron 5585 UTM. The experiment started with the speed compression of 500mm/min, after 80mm of displacement achieve, the experiment is stopped, and specimen is replaced with another one. The process is repeated until all tube composite specimen is tested.

3.6 Crashworthiness Parameter

Crashworthiness is one of the key factors that needs to be considered when evaluating safety of structural components. Besides that, it is apprehensive with the energy absorption through controlled failure modes so that the impact energy is absorbed by progressive manner while maintaining a gradual decay in the load profile. The crashworthiness parameters can be analysed and computed mathematically based on a typical load-displacement history as shown in Figure 3.17.

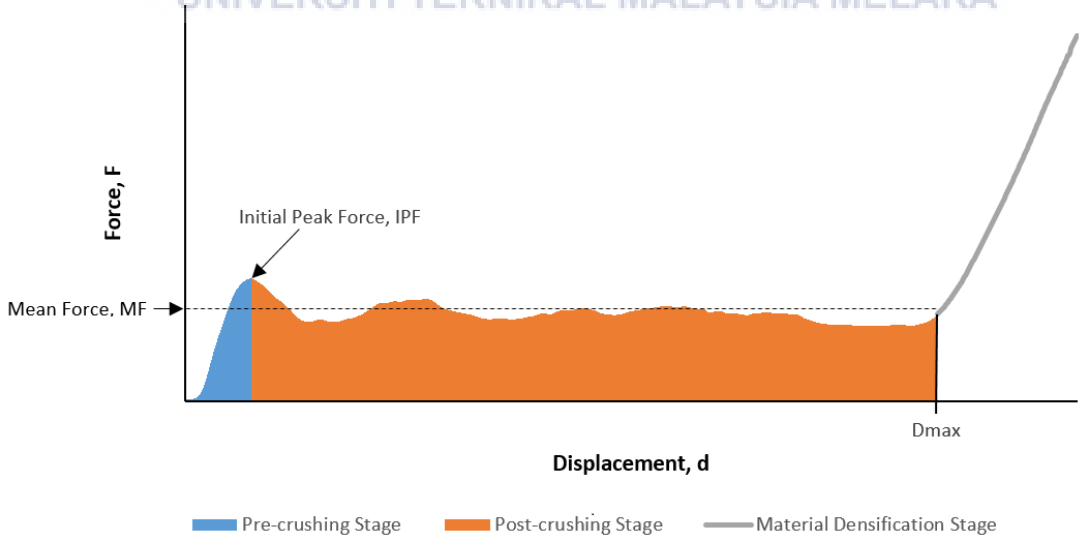

Figure 3.17: Typical Load-Displacement Curve For the composite tube

3.6.1 Initial Peak Load

The initial peak force/load (IPF) is the force required to begin deformation of a plastic tube. The initial peak force should be kept low to limit the risk of passenger harm by reducing the size of reaction forces encountered in situations when safety is critical, such as car and train collisions.

3.6.2 Energy Absorption and Specific Energy Absorption

The ability of composite constructions to absorb crushing energy caused by collisions is measured using energy absorption. The total of the areas under the force-displacement curve for the pre-crush and post-crush regions, i.e. the shaded area in Figure 3.17, represents this quantity graphically. The energy absorbed (EA) is represented mathematically in Equation (1).

$$EA = \int_0^{Dmax} Fds \tag{1}$$

The compressive load is represented by F (N). Equation (2) offers the specific energy absorption (SEA) as a measure of the absorbed energy about the mass of the structure. Dmax is the displacement of the composite structure at the beginning of densification stage.

$$SEA = \frac{EA}{m} \tag{2}$$

where m (kg) is the mass of the specimen.

3.6.3 Mean Crushing Force

The average force that a composite structure experiences when compressed is known as the mean crushing force (MCF) or mean load (Pmean). The calculation excluding forces experienced in the densification stage in Equation (3).

$$MCF = \frac{EA}{Dmax} \tag{3}$$

Hence, Dmax is the displacement of the composite structure at the beginning of densification stage.

3.6.4 Crush Force Efficiency

Crush force efficiency (CFE) quantifies the ratio of the mean force experienced by the composite and to its initial peak crushing force Equation (4).

$$CFE = \frac{Pmean}{Pmax} \tag{4}$$

Pmean is the mean load and Pmax in the maximum peak value, mostly on typically for load-displacement composite tube test, the Pmax is equal to the initial peak value. In terms of energy absorption, an optimum scenario is attained when CFE is 1, which implies that the initial peak crushing force is maintained during the entire post-crushing period and is about equivalent to the mean crushing force

3.7 Data Analysis

The results that are obtained in the compression test will further be analysed. To make comparisons easier, the data will be presented as graphs and tables. The average of each crashworthiness parameter properties for each test from the various type of composite tube that have different degree orientation of fibreglass with different trigger mechanism, no

chamfer (NC) and 45º internal single chamfer (SC). To be studied. At the end of the analysis and report writing, the best orientation degree of fibre glass and type of trigger mechanism that have superior in crashworthiness parameter will be stated. Appendix A, show the raw data and graph that generated by the Bluehill software.

CHAPTER 4

RESULT AND DISCUSSION

4.1 Introduction

In this chapter, the experimental data and result for mechanical properties of the compression test for the PVC tube reinforced with the GFRP is shown. In this research, the quasi-static compression test is used to collect data for the energy absorption and crashworthiness parameter from the graph produce by the test. The test has four types of fibre orientation with two types of trigger mechanism. Table 4.1 show the detail of the specimens.

Table 4.1: Detail no of specimen

Type.	Fibreglass Orientation (º)	No Trigger (NC)	45º Internal Single Chamfered (SC)
A	No fibreglass	3	3
B	0º/90º	3	3
C	-30º/60º	3	3
D	-45º/45º	3	3

4.2 Quasi-Compression Test

In the experiment, the INSTRON 5585 UTM is utilised to complete the quasi-compression test. The test was run and the crosshead speed rate is at 500mm/min at constant speed. The displacement for this compression test is stop when the displacement achieves 80mm.In this experiment all the data and result for the specimen was taken and the data were collected.

4.3 Physical Properties of The Specimen

The physical properties for the specimen including the inner diameter, outer diameter, the wall thickness and the length of the specimen is shown in Table 4.2.

Table 4.2: Physical properties for specimen

No.	Type of Specimen	Inner Diameter(mm)	Outer Diameter(mm)	Wall Thickness (mm)	Length (mm)	Mass(g)
1	ANC1	53	60	7	98	91
2	ANC2	53	60	7	98	93
3	ANC3	53	60	7	98	91
4	ASC1	53	60	7	98	90
5	ASC2	53	60	7	98	91
6	ASC3	53	60	7	98	92
7	BNC1	53	63	10	98	140
8	BNC2	53	63	10	98	140
9	BNC3	53	63	10	98	139
10	BSC1	53	63	10	98	141
11	BSC2	53	63	10	98	141
12	BSC3	53	63	10	98	142
13	CNC1	53	64	11	98	154
14	CNC2	53	64	11	98	148
15	CNC3	53	64	11	98	154
16	CSC1	53	64	11	98	148
17	CSC2	53	64	11	98	144
18	CSC3	53	64	11	98	147
19	DNC1	53	63	10	98	147
20	DNC2	53	64	11	98	149
21	DNC3	53	64	11	98	149
22	DSC1	53	63	10	98	150
23	DSC2	53	63	10	98	150
24	DSC3	53	63	10	98	151

4.4 Crushing Behaviour Under Quasi-Compression

4.4.1 PVC Tube Without GFRP.

Figure 4.1(a) show the load-displacement graph corresponding to the image in Figure 4.1(b) for ANC. From the Figure 4.1(a) the straight-line region in which the load is direct proportion to the displacement until reach a local maximum which is initial peak load(iPmax) at 46.522kN with approximately at displacement 5mm. The load value decrease after reach the iPmax due to the folding form at the bottom of the specimen. The specimen undergoes progressive folding as the as the folds continued to form, stresses built up in the tube wall, resulting in a hinge, and the load-bearing capacity of the tube decreased as a result of the folding. With each succeeding fold, the load fluctuated less dramatically, and as a result, the failure was more stable. After reach displacement approximately at 75mm, the densification stage is occurred and the load continuously increase drastically.

Figure 4.2(a) show the load displacement graph corresponding to the image in Figure 4.2(b) for ASC. From the Figure 4.2(a) the load is increase direct proportionally to the displacement until reach the iPmax at about displacement 8mm. After that, the load decrease as the first folding occur at the top region of the specimen. The buckling progressive folding is occurred to the specimen. Stresses built up in the tube walls, resulting in a hinge, and the tube's load-bearing capacity was reduced as a result of the folding. Each fold reduced the load's fluctuation, and the failure became more stable as a result. The densification stage begins when displacement reaches 71mm, and the load steadily increases after that.

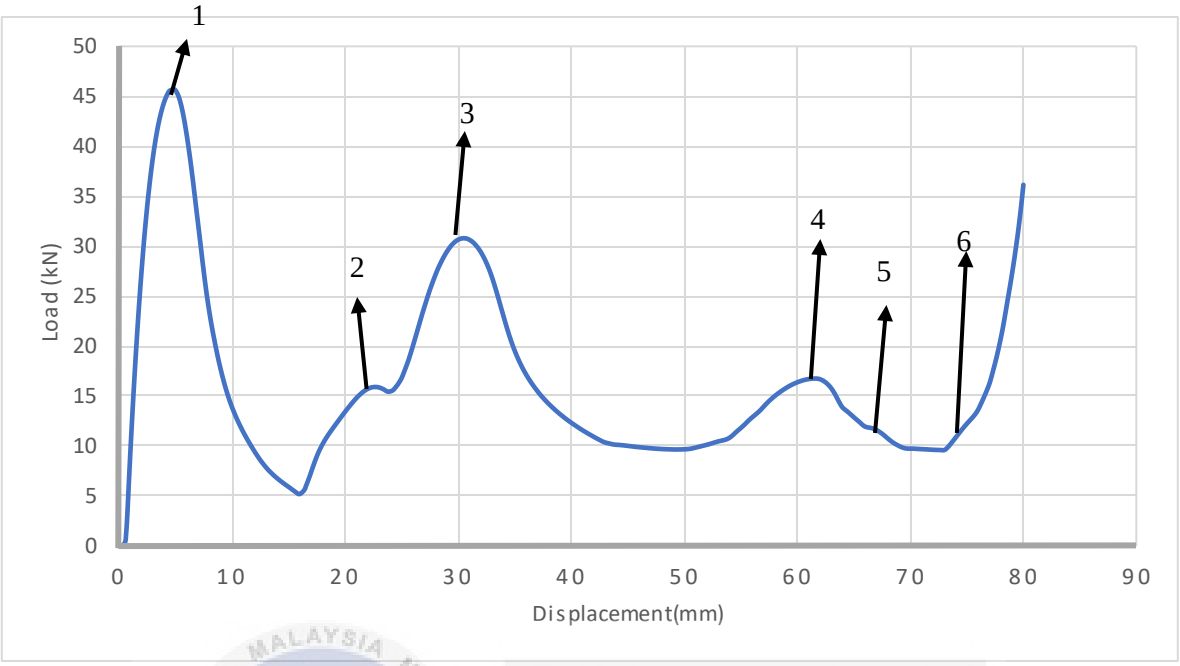

Figure 4.1(a): Load-Displacement Curve for ANC

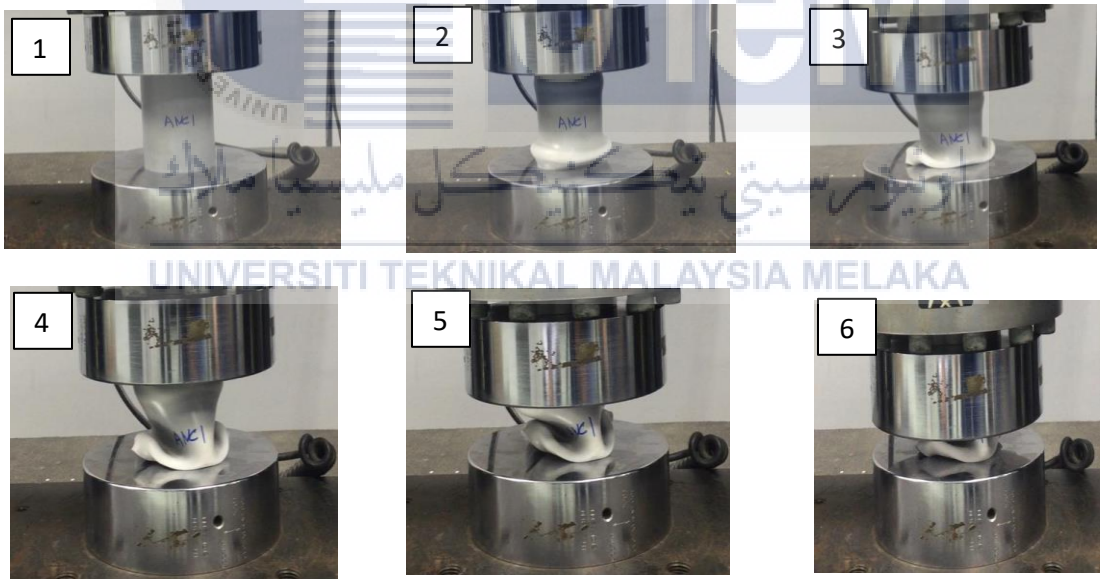

Figure 4.1(b): Compression History for ANC specimen

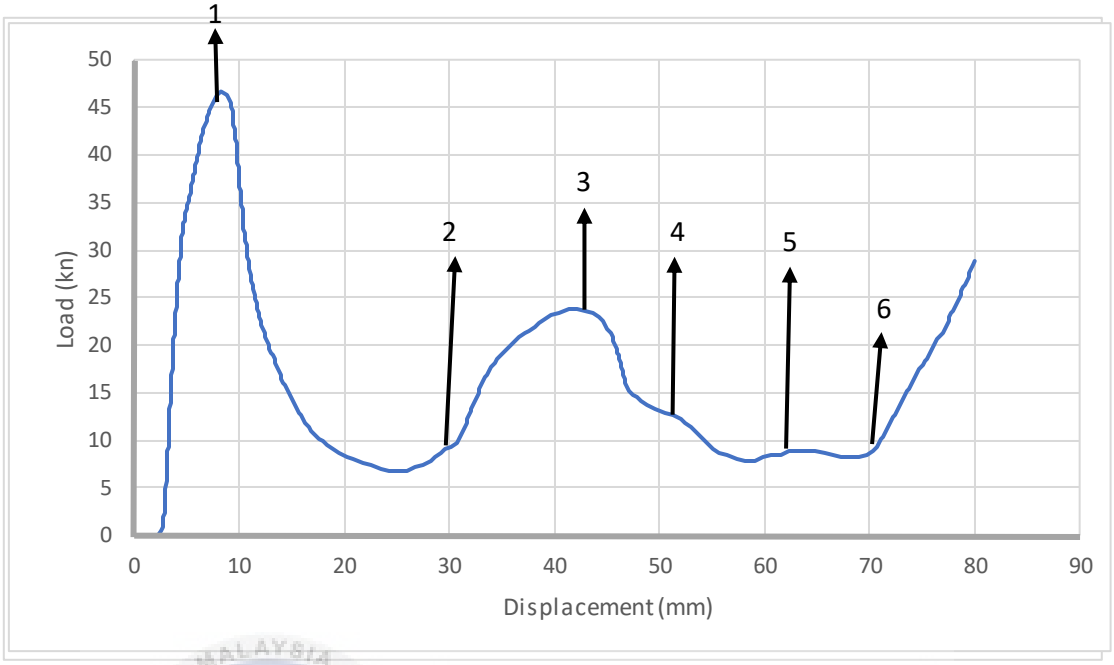

Figure 4.2(a): Load-Displacement Curve for ASC

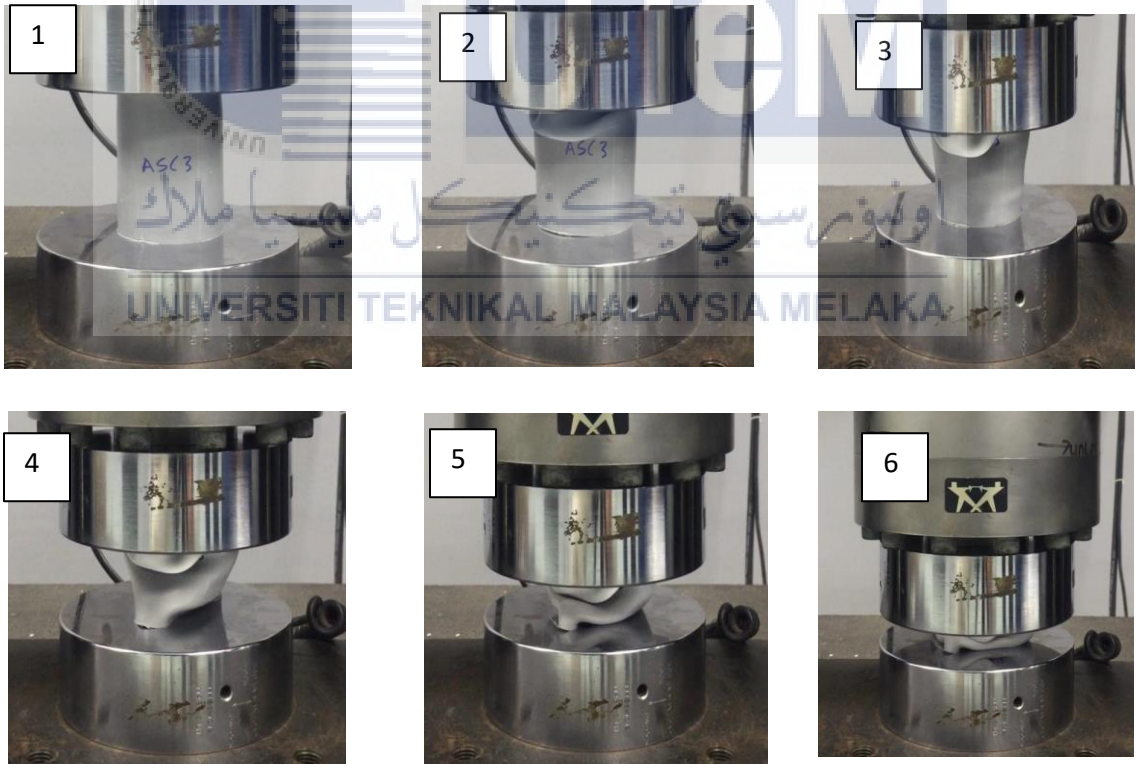

Figure 4.2(b): Compression History for ASC specimen

4.4.2 PVC/GFRP With 0º/90º Orientation.

Figure 4.3(a) show the load-displacement graph and Figure 4.3(b) show the corresponding image of crush history for BNC. The load increase direction proportionally to the displacement until reach the iPmax at displacement approximately 5mm with load 73kN. As the load began to decrease due to the buckling and matrix cracking for the fibreglass to form the folding. Can observe that the fibreglass is hanging out may due to the direction of the fibre orientation is same to the loading direction cause the interpenetration failure. Because the loading direction was normal to the fibre orientation, the fibres provided a higher resistance to compression loading than the other samples, and as a result, a greater load was required to overcome this resistance than the other samples. The densification stage occurs at approximately at 72mm and the load continue to rise.

Figure 4.4(a) show the load-displacement graph and Figure 4.4(b) show the corresponding image of crush history for BSC. The load increase direction proportionally to the displacement until reach the iPmax at displacement approximately 5mm with load 72kN. After some time had passed, the load began to reduce as a result of buckling and fibre cracking, which allowed the fibreglass to begin to fold. It is possible to see that the fibreglass is hanging out, which may be caused by the fact that the direction of the fibre orientation is the same as the loading direction, resulting in interpenetration failure. In part because the loading direction was perpendicular to the fibre orientation, the fibres gave a stronger resistance to compression loading than the other samples, and as a result, a bigger load was required to overcome this resistance than for the other samples as well. It is estimated that the densification stage occurs at 72mm, and the load continues to climb drastically.

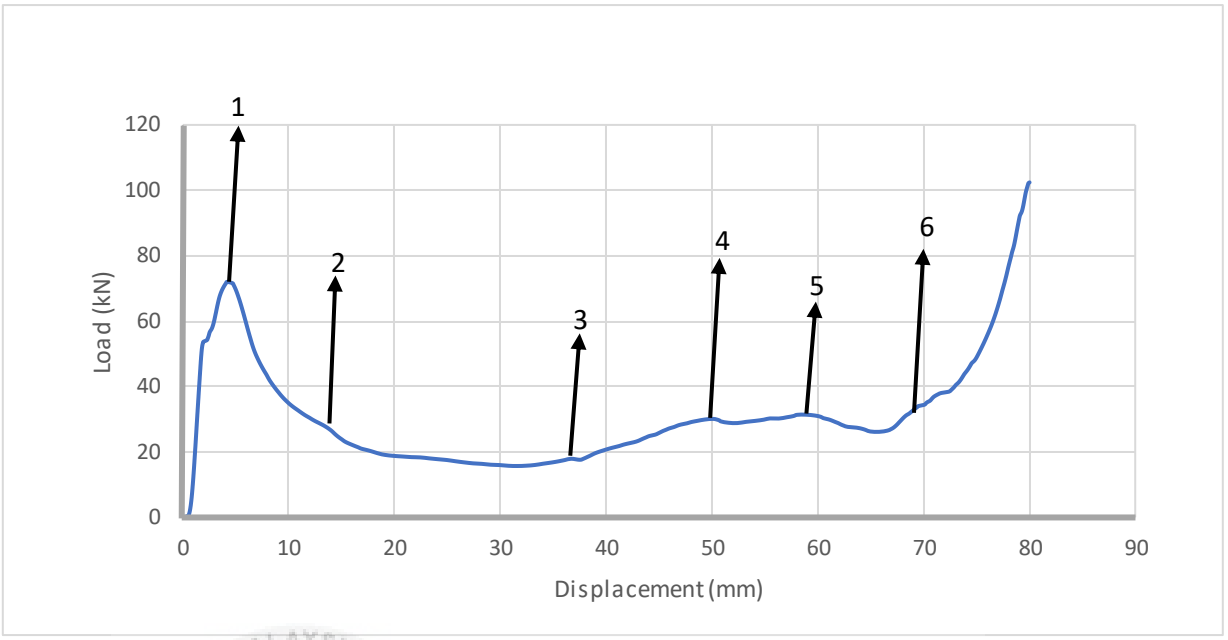

Figure 4.3(a): Load-Displacement Curve for BNC

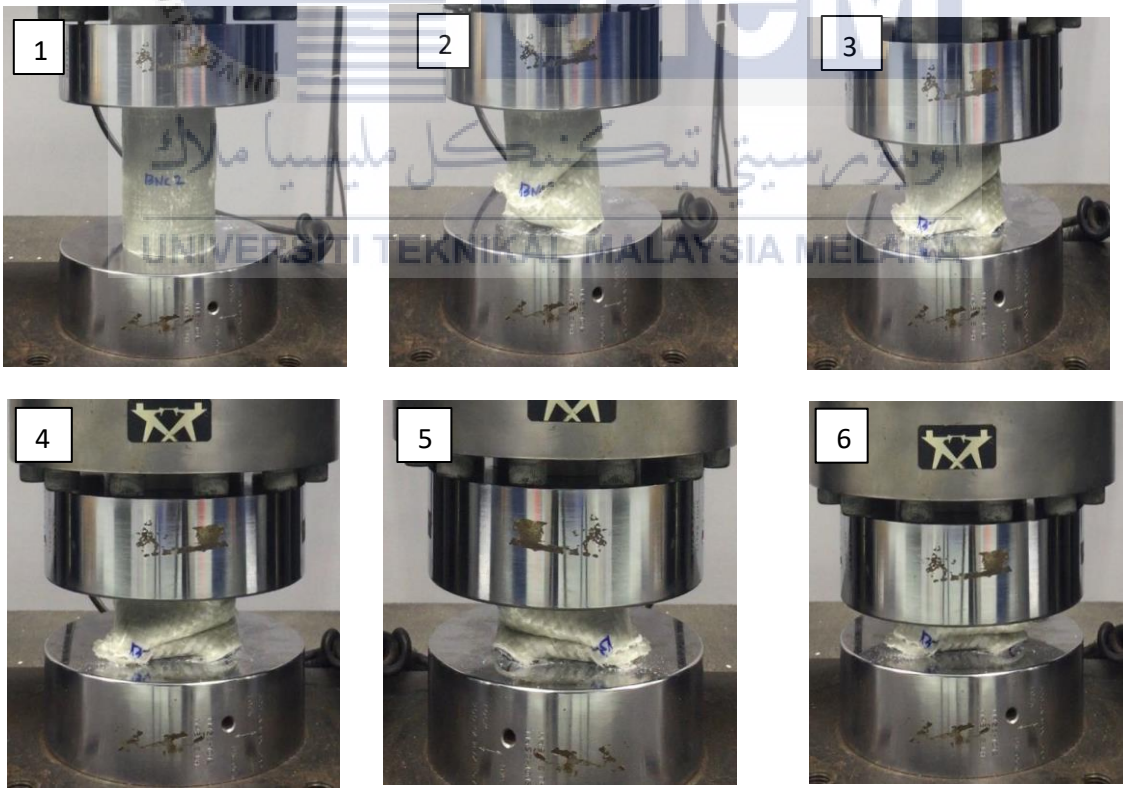

Figure 4.3(b): Compression History for BNC specimen

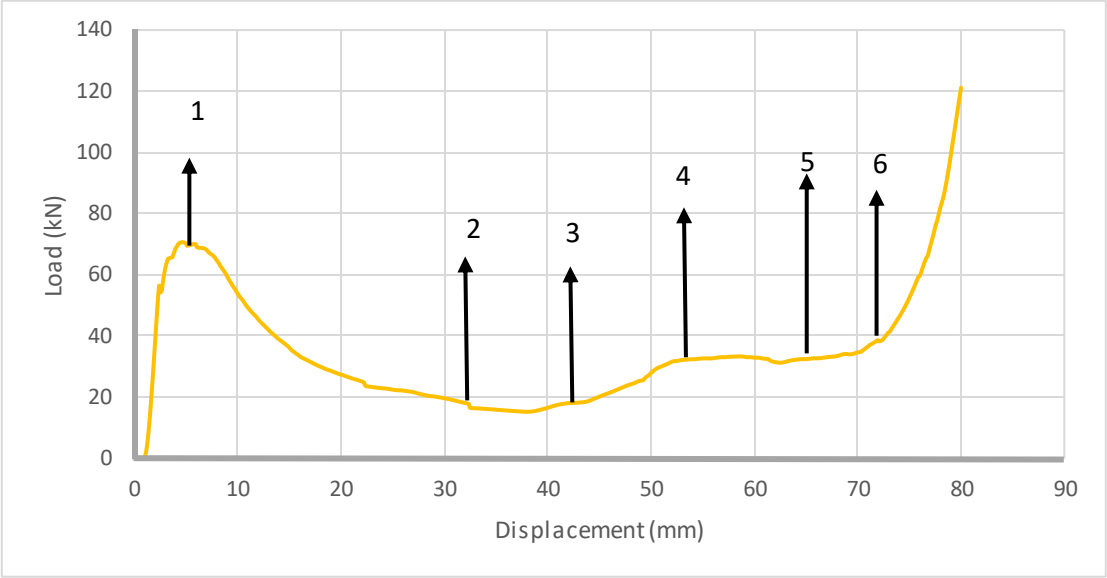

Figure 4.4(a): Load-Displacement Curve for BSC

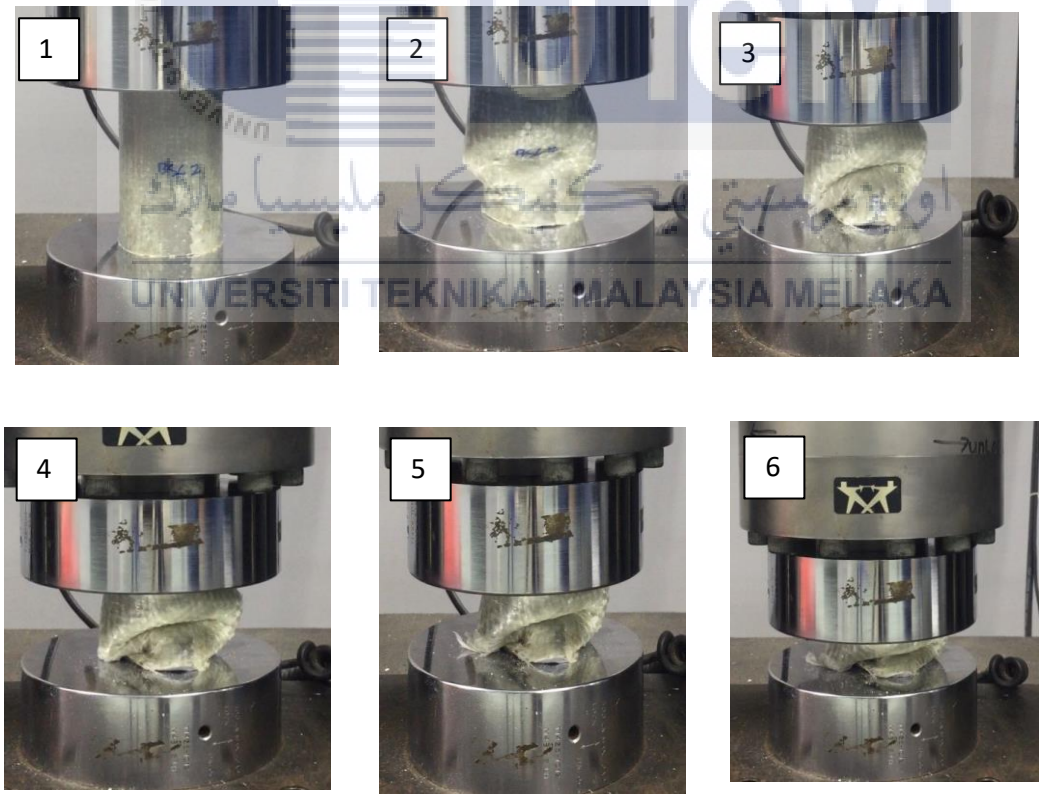

Figure 4.4(b): Compression History for BSC specimen

4.4.3 PVC/GFRP With -30º/60º Orientation.

Figure 4.5(a) show the load-displacement graph corresponding to the image for crush history in Figure 4.5(b) for CNC. The straight-line direct proportion to the displacement as the load increase until reaches iPmax at displacement 5mm with load 74kN approximately. The load continuously decrease as the fold is form from the buckling and the fibre cracking due to the load. The load less fluctuant after the first fold form and the load more stable It was subsequently discovered that both sections of the tube continued to interpenetrate through one another while the matrix cracks formed by the split also grew longer, ultimately lowering the load-bearing capacity of the tube. The densification stage occurs at 70mm and the load continuously rising.

Figure 4.6(a) show the load-displacement graph corresponding to the image for crush history in Figure 4.6(b) for CSC. The straight-line direct proportion to the displacement as the load increase until reaches iPmax at displacement 5mm with load 62kN approximately. The load continuously decrease as the fold is form from the buckling and the fibre cracking due to the load. The load less fluctuant after the first fold form and the load more stable It was subsequently discovered that both sections of the tube continued to interpenetrate through one another while the matrix cracks formed by the split also grew longer, ultimately lowering the load-bearing capacity of the tube. The densification stage occurs at 70mm, and the load continues to rise throughout the process.

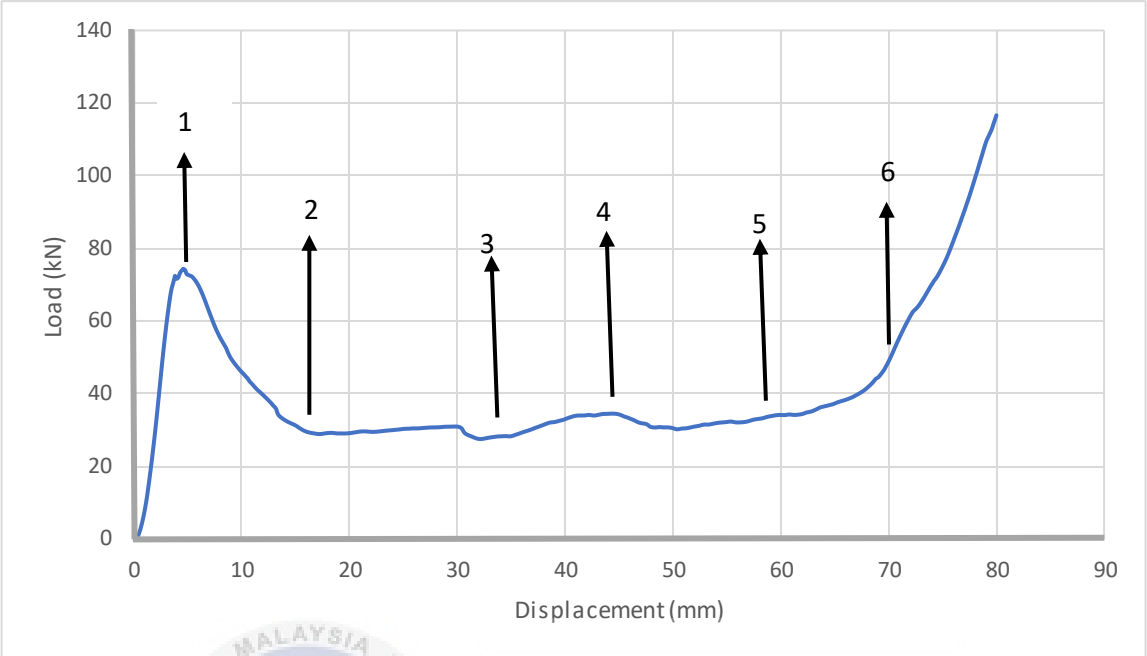

Figure 4.5(a): Load-Displacement Curve for CNC

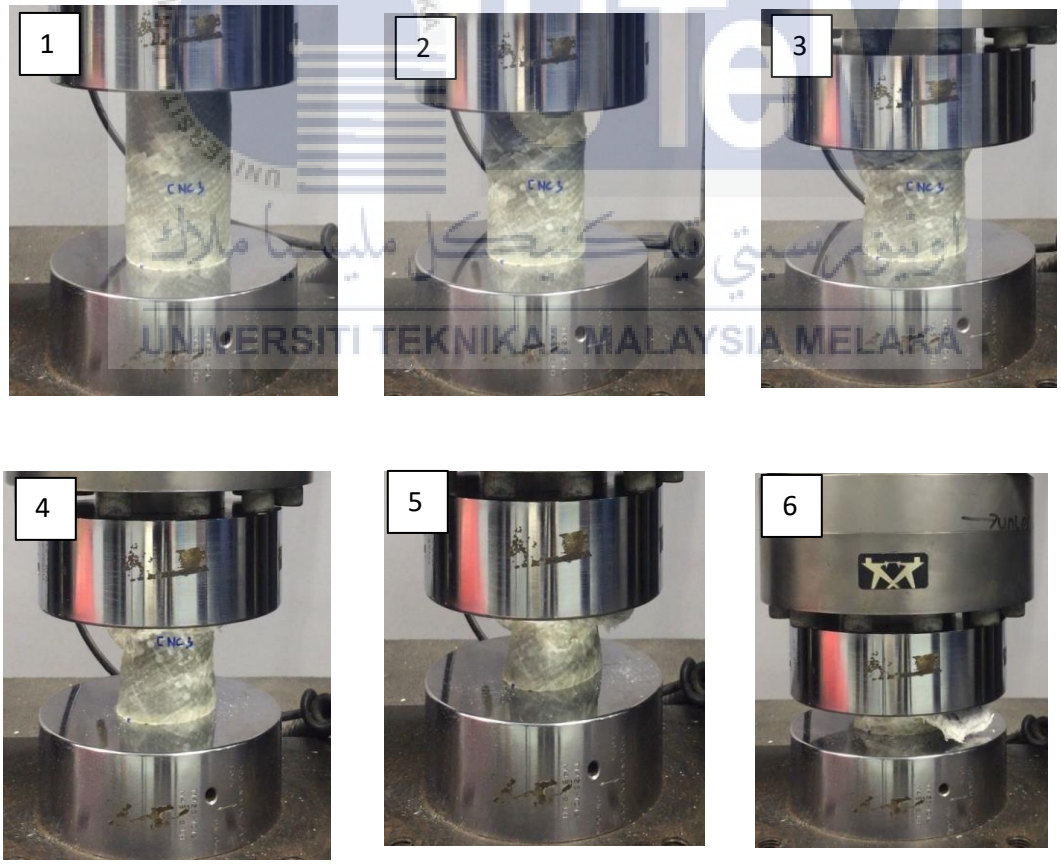

Figure 4.5(b): Compression History for CNC specimen

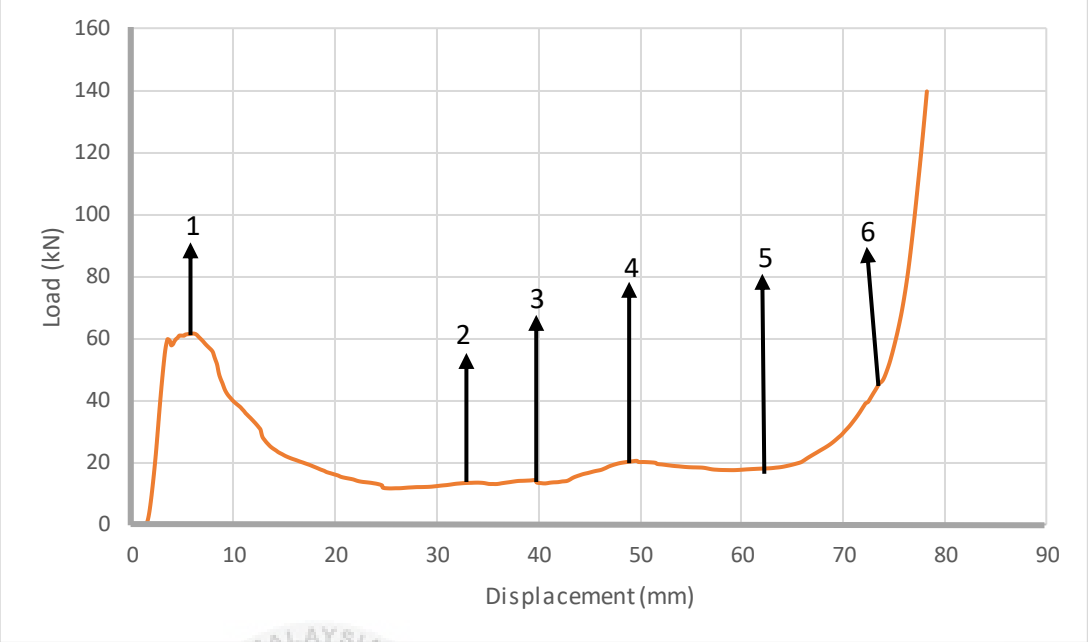

Figure 4.6(a): Load-Displacement Curve for CSC

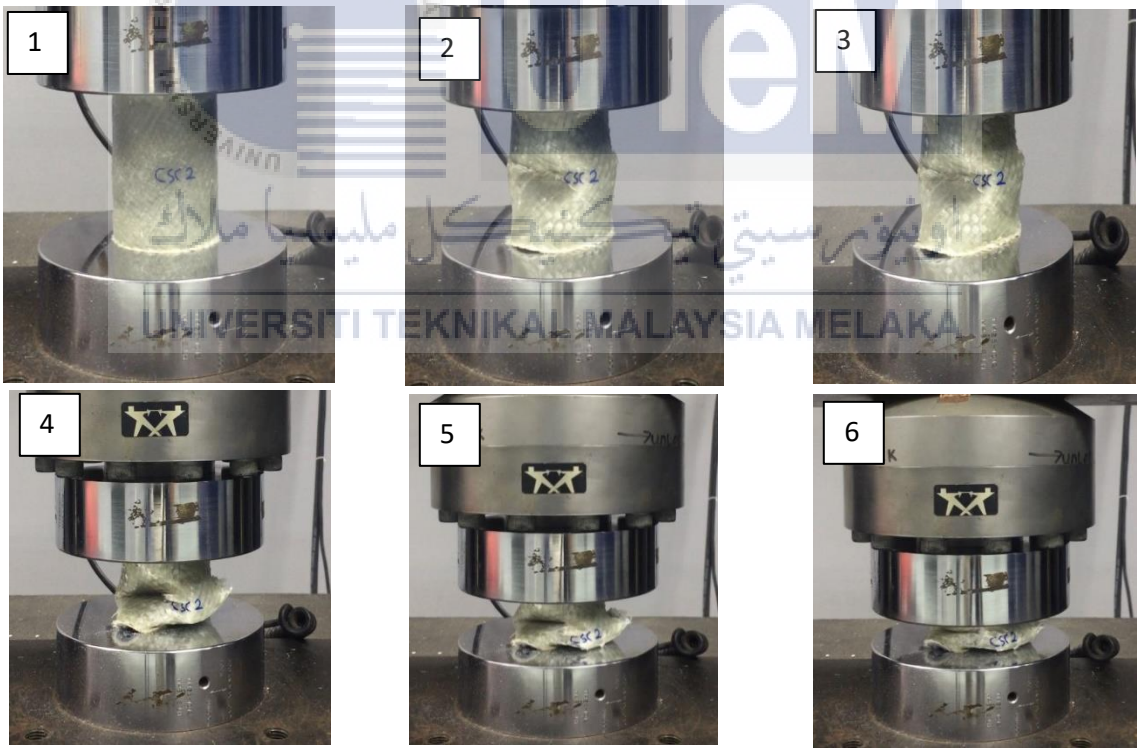

Figure 4.6(b): Compression History for CSC specimen

4.4.4 PVC/GFRP With -45º/45º Orientation

Figure 4.7(a) show the load-displacement graph corresponding to the image for crush history in Figure 4.7(b) for DNC. The straight-line direct proportion to the displacement as the load increase until reach iPmax at displacement 5mm with load 74kN approximately. The load continuously decrease as the fold is form from the buckling and the fibre cracking due to the load. The buckling, matrix cracking, and final collapse of the DNC composite tube resulted in significant damage to the tube, but the adhesion between the GFRP and the PVC inner tube was observed to be intact as the two components of the composite tube remained joined together and did not separate. Delamination during failure was also minimal, as evidenced by the fact that even after densification, there were no obvious dangling loose bunches of the GFRP to be found. The densification stage occurs at 76mm and the load continuously rising.

The load-displacement graph in Figure 4.8(a), which corresponds to the image for crush history in Figure 4.8(b) for DSC. As the load increases, the straight-line direct proportion to the displacement increases until it reaches iPmax at a displacement of 10mm and a load of approximately 71kN. The load decreases continually when the fold is formed as a result of the buckling and the fibre breaking as a result of the stress. The buckling, matrix cracking, and final collapse of the DSC composite tube caused significant damage to the tube, but the adhesion between the GFRP outer tube and the PVC inner tube was observed to be intact because the two components of the composite tube remained joined together and did not separate during the test procedure. Even after densification, no evident dangling loose bunches of GFRP could be seen, which indicates that delamination during failure was kept to an absolute minimum. The densification stage occurs at 72mm, and the load continues to rise throughout the process.

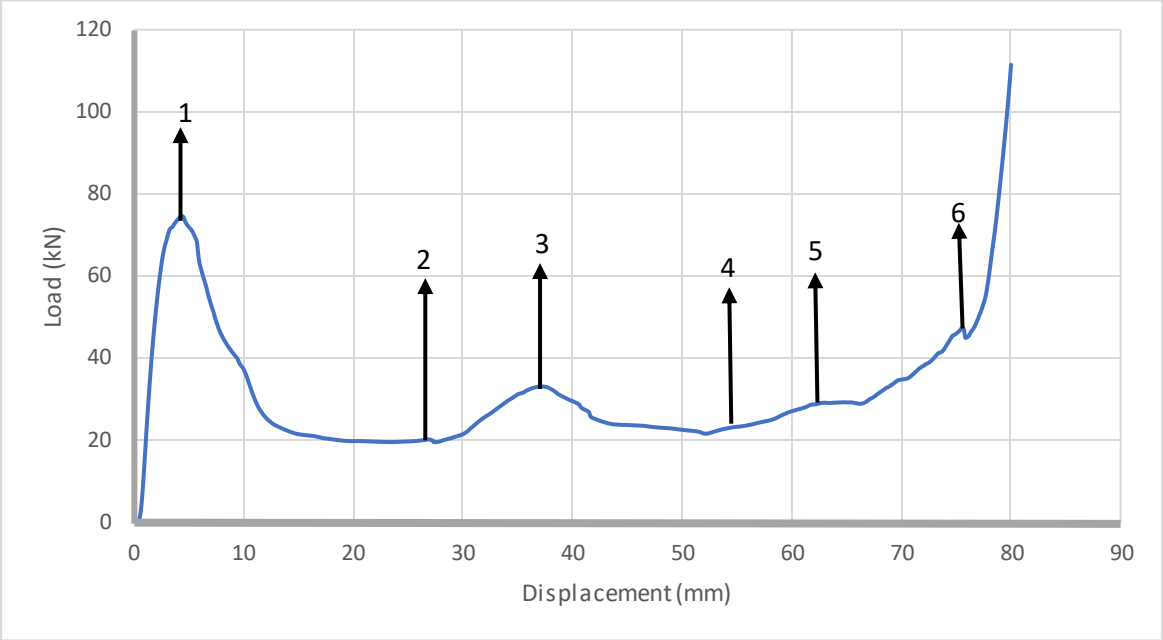

Figure 4.7(a): Load-Displacement Curve for DNC

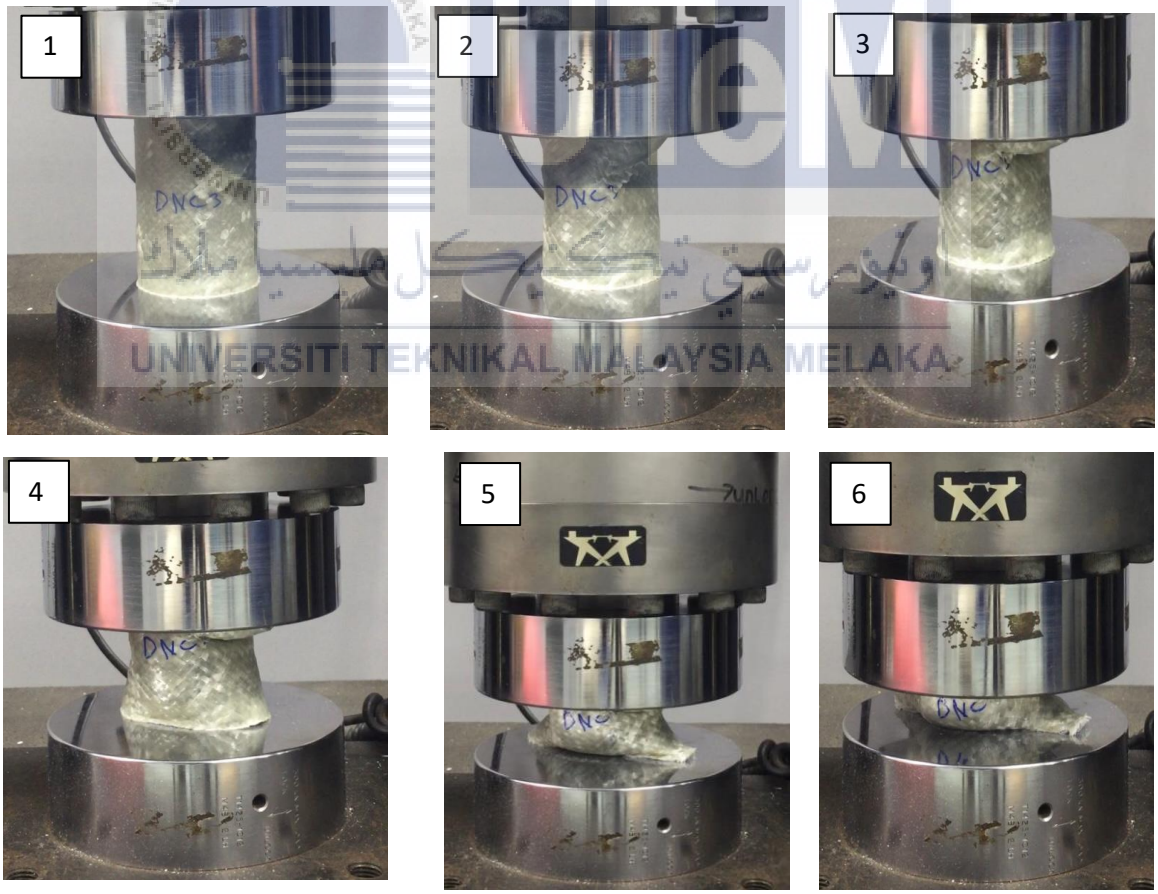

Figure 4.7(b): Compression History for DNC specimen

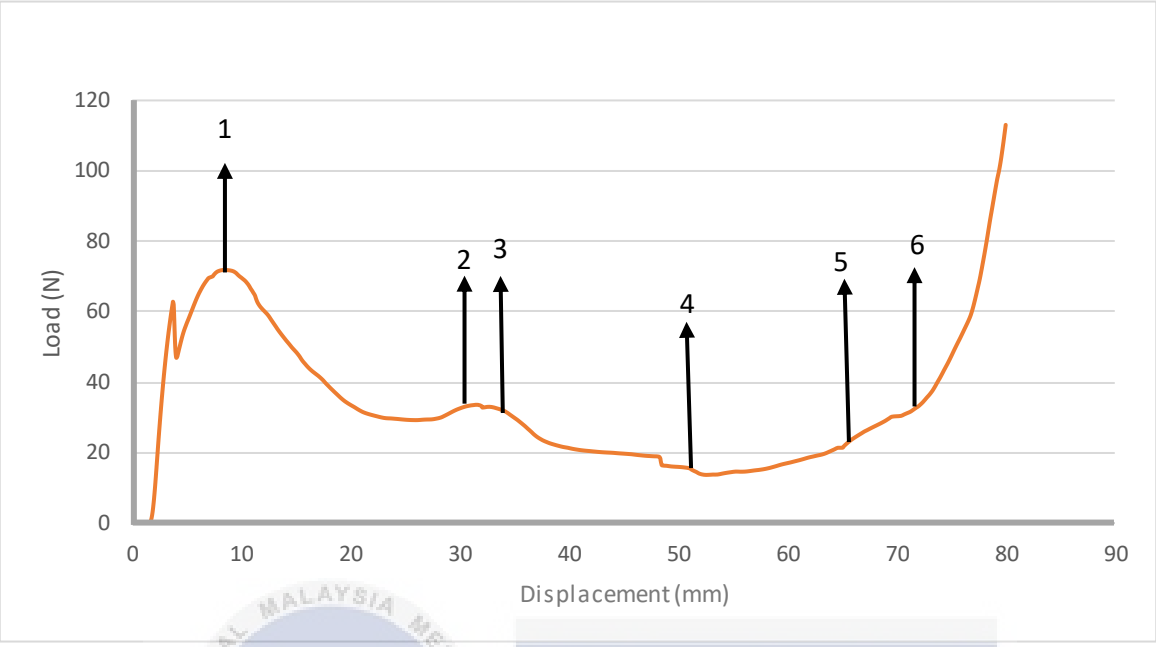

Figure 4.8(a): Load-Displacement Curve for DSC

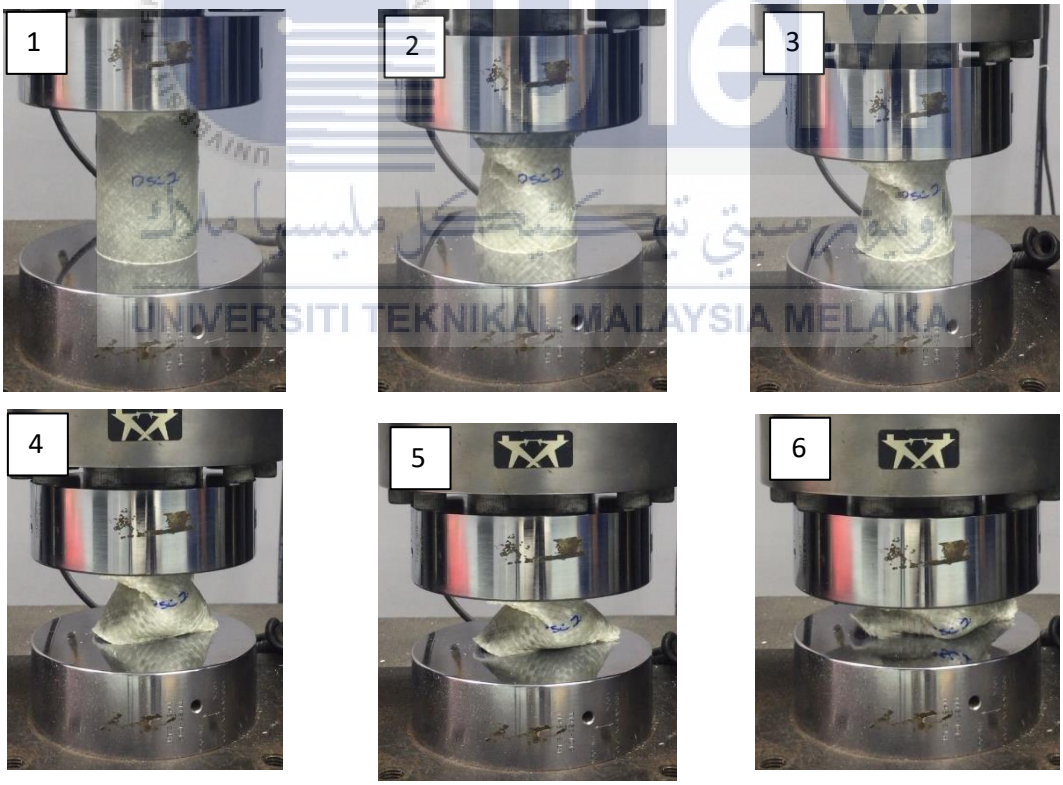

Figure 4.8(b): Compression History for DSC specimen

.

4.5 Crashworthiness Characteristic

From the experimental result, the crashworthiness parameter can be obtain including energy absorption (EA), specific energy absorption (SEA) and crush force efficiency (CFE) by utilized the data from the INSTRON 5585 UTM. Table 4.3 show the detail result for the crashworthiness characteristic.

Table 4.3: Crashworthiness parameter characteristic result

Type	Initial Peak Load(kN)	Mean Load (kN)	Energy Absorption(kJ)	Specific Energy Absorption (kJ/kg)	Crush Force Efficiency (CFE)
ANC	46.522±1.115	20.517±0.042	1.123±0.118	12.244±1.177	0.441±0.01
ASC	42.805±4.558	21.325±0.112	1.299±0.292	14.332±3.221	0.503±0.061
BNC	73.053±1.038	40.707±3.590	2.39±0.408	17.116±2.955	0.557±0.041
BSC	72.168±1.563	38.877±3.602	2.189±0.211	15.483±1.431	0.538±0.039
CNC	74.246±3.448	38.020±4.320	2.212±0.422	14.512±2.475	0.511±0.038
CSC	65.535±3.656	32.447±4.874	1.725±0.35	11.772±2.254	0.494±0.05
DNC	74.035±0.850	37.911±1.880	2.199±0.39	14.84±2.758	0.512±0.031
DSC	71.392±0.980	38.369±0.239	2.281±0.121	15.175±0.768	0.537±0.004

4.5.1 Initial Peak Load

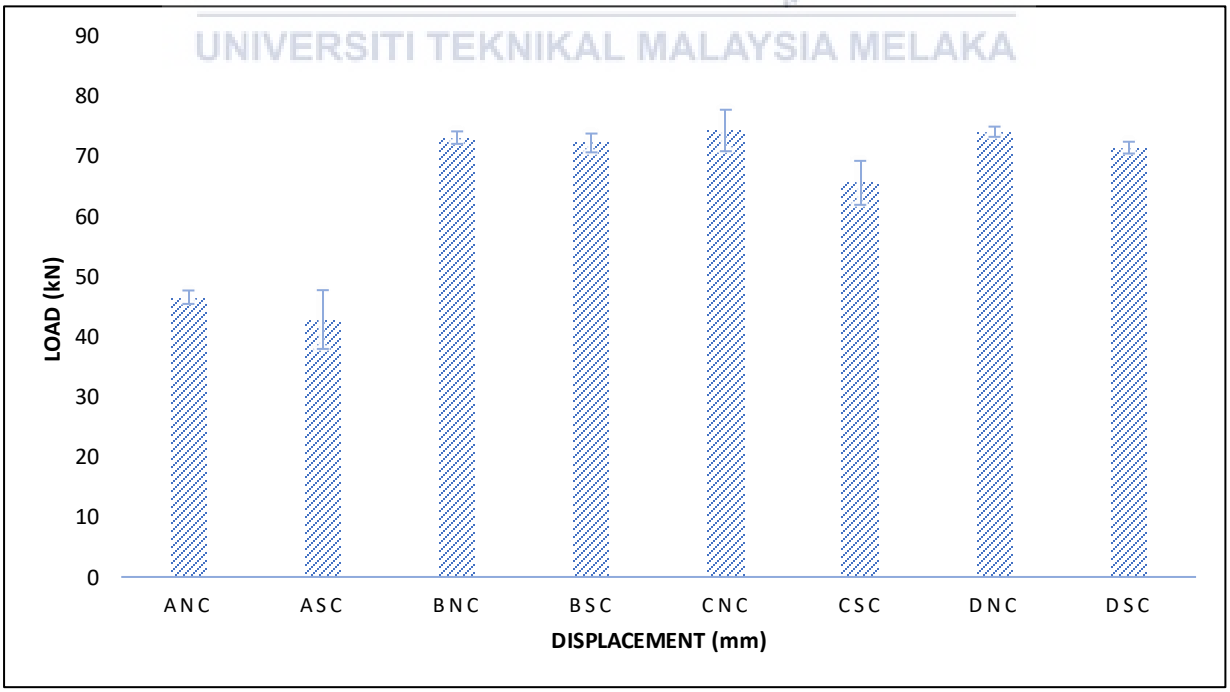

Figure 4.9: Initial Peak load comparison for all type of specimen

The initial peak load (iP*max*) is the force that needed for the specimen to have first deformation stage. In the Figure 4.9 show that the no chamfer (NC) type of specimen have higher initial peak load than the 45º single chamfer (SC). For type A specimen, the decrement of peak load from ANC and ASC is about 8.05% from the peak load 46.552kN to 42.805kN. As for the type B, from BNC to BSC have the decrement of 1.211% with value from 73.053kN to 72. 168kN.The type C also show the decrement pattern with 11.733% decrement with CNC value of 74.246kN and CSC value with 65.535kN. For the type D. the DNC value show the peak load value at 74.035kN and the DSC value at 71.392kN with decrement 3.57%. From the result for peak value, this satisfies with the previous study on. notch trigger, effect of trigger, where Nasir Hussain et al.,(2021).and Sivagurunathan et al.,(2018b) stated that the peak value of the composites tube decrease by using trigger mechanism. Besides, this confirmed that by using trigger can reduce the peak load value for the composite. In sum, by using trigger SC would minimize the initial peak crush load value of magnitude during the crushing event than the NC type.

The orientation of the fibreglass also influences the peak load value for the specimen. In Figure: 4.9, the 0º/90º (B), -30º/60º(C) and -45º/45º(D) specimen show the higher initial peak load value than the no fibreglass(A) specimen. As the for the NC type of trigger, the C (74.246kN) have the highest peak value than D (74.035kN) and B (73.035kN). This contradicted with the previous study on. PVC/GFRP tube, where Khan et al., (2021), stated that the initial peak load value is higher due to the increase of angle orientation have same direction to the direction of the loading. This occur due to, in the study by Khan et al., (2021), use unidirectional fibreglass while in this study use plain weave fibreglass. In SC type, the C (65.535kN) have the lowest peak compared to B (72.168kN) and D (71.392kN), this occur may to the imperfect fabrication due to surrounding and other cause, it is supposed to follow the pattern for the NC type.

4.5.2 Mean Load

Mean load P*mean* is the measure to compare the overall energy absorption performance of the composites, Figure 4.10 show mean load comparison for the specimen.

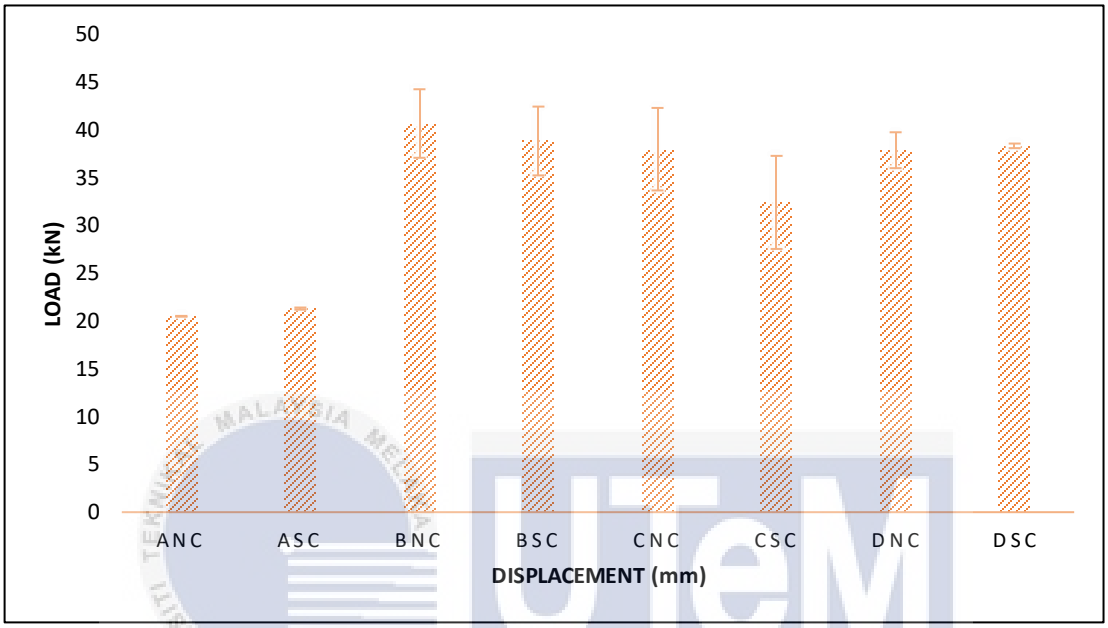

Figure 4.10: Comparison mean load for the specimen

From the figure 4.10, the all PVC/GFRP (B, C and D) have the higher mean load value from the PVC tube (A) itself. For the NC type of specimen slightly have higher the mean load value than the SC. Thus, agreed with the previous study (e.g. Crushing and energy absorption mechanisms of carbon fiber-epoxy tubes under axial impact), by Ataabadi et al., (2019), stated that from the result, the NC exhibit the large mean load value than the tube with the trigger mechanism. Beside, from the Figure 4.10, the type of NC specimen that have the higher mean value is BNC (40.707kN) and for the CNC (38.02kN) slightly higher than DNC (37.911kN), in summary the best way to increase PVC/GFRP composite tube mean load values while improving crush stability is to apply NC type of trigger.

From Figure 4.10, the 0º/90º (B) type of specimen have superior mean load value than the other type of specimen, followed by -30º/60º (C) and -45º/45º(D). and contradict

from the previous study on winding orientation for hybrid and non-hybrid composite tube, Supian et al., (2021), stated that the P*mean* values decreased with the increase in the winding orientations. This may occur due to the different fabrication method and the pattern type of the glass fibre glass. B type show the best result for both BNC (40.707kN) and BSC (38.877kN) type of specimen. Hence, B is the optimum orientation to achieve maximum value of the mean load.

4.5.3 EA and SEA

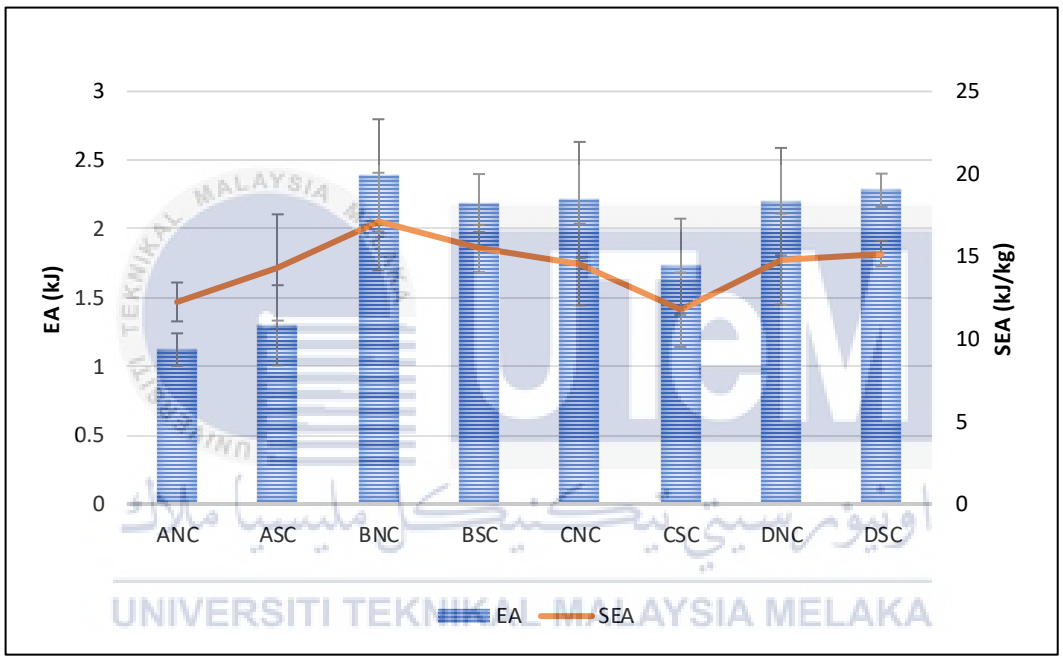

Figure 4.11: Comparison SEA and EA for the specimens

The area under the graph of a load displacement curve from 0mm to 70mm is used to calculate total energy absorption (EA). From Figure 4.11, the PVC/GFRP tubes specimen have higher value in term of EA, BNC has the highest value at 2.39 kJ. When compare between NC and SC types of specimen, BNC (2.39 kJ) have the higher EA than the BSC (2.189 kJ) with different value 0.201 kJ. Besides, for the CNC (2.212 kJ), it has higher value than CSC (1.725 kJ) with differences 0.487 kJ. For the D and A type of specimen, the SC slightly higher than NC which is DSC (2.281 kJ) slightly higher than DNC (2.199 kJ) with value different 0.082 kJ and ASC (1.299 kJ) slightly higher than ANC (1.123 kJ) with 0.176

kJ different. The B and C that NC higher than SC types of specimen shows the huge value different (B=0.201 kJ, C=0.487 kJ) compare to A and D specimen that having SC slightly higher than NC with value different (A=0.176 kJ, D=0.076 kJ). Thus, the NC have good energy absorbing than the SC trigger mechanism. This satisfied the previous study (e.g. Crushing and energy absorption mechanisms of carbon fibre-epoxy tubes under axial impact), Ataabadi et al.,(2019), stated that from the result, the no trigger exhibit the large EA value than the having the trigger mechanism but contradict from (e.g. Square tube and circular tube with different trigger mechanism using jute/epoxy) from the Sivagurunathan et al.,(2018a),(2018b), show that the trigger mechanism have better EA value than the no trigger. This may occur due to the Sivagurunathan et al., (2018a) (2018b) use natural fibre as the while from the Ataabadi et al., (2019) that use synthetic fibre same as in this study using synthetic fibre. In conclusion, the no trigger mechanism achieves high EA value than the single chamfer trigger.

As for the orientation fibre, from the Figure 4.11 show the BNC (2.39 kJ) have higher value of EA than the other NC (ANC, CNC, DNC) and BSC (2.189 kJ) also show the second highest value of EA after DSC among the SC. This is because the mass of the DSC slightly more than the BSC due to the DSC have slightly longer than BSC. This satisfied from the previous study on. PVC/GFRP tube, where Khan et al., (2021), show that the higher the orientation degree of the fibreglass, the higher the EA value for the PVC/GFRP composite tube. In conclusion, the B ($0^o/90^o$) orientation of fibreglass give the highest value for the EA.

Especially relevant when comparing the energy absorption capabilities of different types of energy absorbers made from various materials and masses is the use of specific energy absorption (SEA). Typically, the greater the value of the SEA, the more efficient the energy absorber is considered to be. From the Figure 4.11, the PVC/GFRP tubes specimen have higher value in term of SEA. BNC has the highest value at 17.116 kJ/kg. When compare

between NC and SC types of specimen, BNC (17.116 kJ) have the higher SEA than the BSC (15.483 kJ/kg) with different value 1.633 kJ/kg. Besides, for the CNC (14.512 kJ/kg), it has higher value than CSC (11.772 kJ/kg) with differences 2.74 kJ/kg. For the D and A type of specimen, the SC slightly higher than NC which is DSC (15.175 kJ/kg) slightly higher than DNC (14.84 kJ/kg) with value different 0.335 kJ/kg and ASC (14.332 kJ/kg) slightly higher than ANC (12.244 kJ/kg) with 2.088 kJ/kg different. The B and C that NC higher than SC types of specimen shows the huge value different (B=1.633 kJ/kg, C=2.74 kJ/kg) compare to A and D specimen that having SC slightly higher than NC with value different (A=2.088 kJ/kg, D=0.335 kJ/kg). Thus, the NC have good specific energy absorbing than the SC trigger mechanism for certain fibre orientation. This satisfied the previous study, Crushing and energy absorption mechanisms of carbon fibre-epoxy tubes under axial impact, Ataabadi et al., (2019), stated that from the result, the no trigger exhibit the large SEA value than the sample with trigger mechanism.

Besides that, the orientation degree of fibreglass also significantly improves the SEA value. In the Figure 4.11 that represent the SEA for the 4 type of the specimen(A,B,C,D), with 2 different trigger (NC,SC) show that the BNC (17.116 kJ/kg) have the highest value followed by the DNC (14.84 kJ/kg) , CNC (14.512 kJ/kg) and ANC (12.244 kJ/kg) for the no trigger (NC) type. As for the single chamfer (SC), BSC (15.483 kJ/kg) have the highest value followed by the DSC (15.175kJ/kg), ASC (14.332 kJ/kg) and CSC (11.772 kJ/kg). The CSC supposedly have higher SEA than the ASC due to have the GFRP to enhance the PVC tube, in the study ASC show the higher value of SEA than the CSC may occur to the GFRP did not stick properly to the PVC tube due to the air bubble presence during the fabrication process and due to the less amount of matrix used in the fabrication process. In conclusion for SEA, the B type that have the highest value of SEA for NC and SC.

4.5.4 Crush Force Efficiency

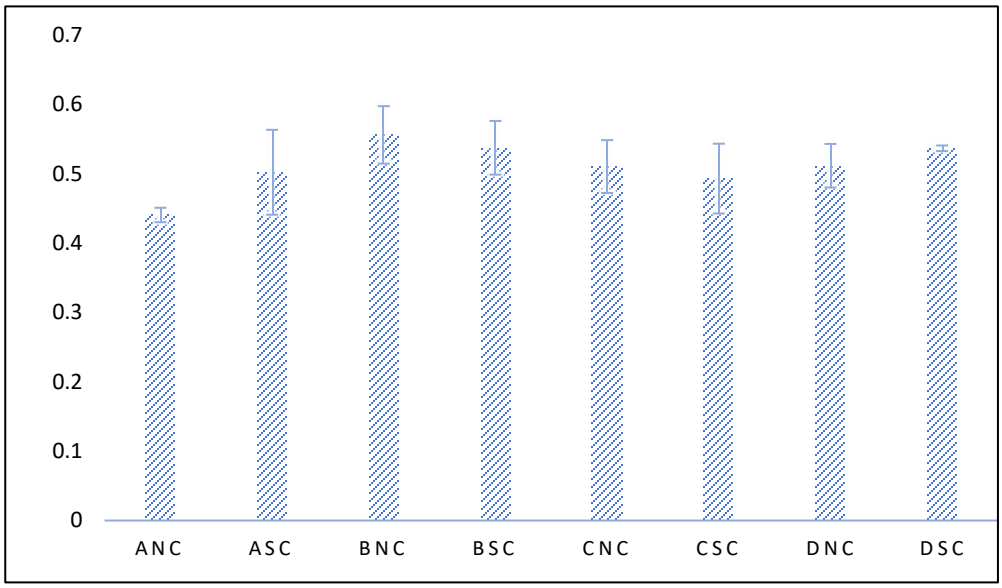

Figure 4.12: Comparison CFE for the specimens

Crush force efficiency (CFE) is a crucial component in evaluating the performance of total energy absorbed and measuring the stability of the crushing process. It is preferable to obtain a high CFE value that is close to unity in order to obtain a good energy absorbing characteristic. CFE can be obtain by utilising the mean load (Pmean) divided max load (Pmax). From the Figure 4.12, show that the PVC/GFRP tubes specimen have higher value of CFE than the PVC tube. When compare between NC and SC types of specimen, BNC (0.557) have the higher CFE than the BSC (0.538) with different value 0.019. Besides, for the CNC (0.511), it has higher value than CSC (0.494) with differences 0.017. For the D and A type of specimen, the SC slightly higher than NC which is DSC (0.537) slightly higher than DNC (0.512) with value different 0.025 and ASC (0.503) slightly higher than ANC (0.441) with 0.062 different. In this study, the NC type at B have the highest CFE value thus make the no trigger has the ideal CFE value contradicted from the previous study by Sivagurunathan et al., (2018a), state that the trigger mechanism has the high CFE value that using external single chamfer while in this study using internal single chamfer.

Besides that, the orientation degree of fibreglass also significantly improving in the CFE value. In the Figure 4.12 that show the CFE value for the 4 type of the specimen(A,B,C,D), with 2 different trigger (NC,SC) show that the BNC (0.557) have the highest value followed by the DNC (0.512), CNC (0.511), and ANC (0.441) for the no trigger (NC) type. As for the single chamfer (SC), BSC (0.538) have the highest value followed by the DSC (0.537), ASC (0.503) and CSC (0.494). From the result of CFE, B has the highest CFE value for NC and SC types of trigger. Thus, this satisfy with the previous study (e.g. PVC/GFRP tube) where Khan et al., (2021), show that the CFE value at 90º is greater than the lower degree orientation. We can conclude that, the type B have the highest of CFE value for both NC and SC type of trigger.

CHAPTER 5

CONCLUSION AND RECOMMENDATION

5.1 Conclusion

In this study, the PVC/GFRP composites were subjected under axal-compression test to determine the fibre orientation and trigger mechanism effect to the crashworthiness parameter properties. While, the use of trigger mechanism slightly increases the Pmean and CFE for type A and D but decrease for type B and C. Thus, for the iPmax in this study satisfy with previous study that the trigger mechanism can reduce the peak load for tube composite. However, the trigger mechanism shows better absorption capability for type A and D while significantly poor for type B and C. and by using trigger mechanism can reduce the peak load value. From the result, the best ideal option is to use trigger mechanism to reduce significantly the initial peak load while slightly reducing energy absorption and specific energy absorption capability for certain type of fibre orientation configuration.

. The PVC/GFRP tube composite show the better result than the PVC tube alone. Thus, the PVC/GFRP composite tube with fibre orientation with B ($0^o/90^o$) show the better crashworthiness parameter value for the Pmean, EA, SEA and CFE perspectives. From the EA and SEA parameter, the B type have the highest energy absorption capability that the C and D type. In sum, the fibre orientation may affect with the trigger mechanism geometry due to the different result for NC and SC for 4 type of fibre orientation. Overall, the fibre orientation B($0^o/90^o$) show the best result for crashworthiness parameter, the D($-45^o/45^o$) type is exceptional have best crashworthiness parameter second from B. Thus, hopefully the findings of this experimental study could assist engineers and manufacturers build a crashworthy structure more effectively.

5.2 Recommendation

This current research can be further improved in the future by incorporating additional types of natural fibres, such as coir, kenaf, sisal, flax, and cotton, into the process. Natural fibres, on the other hand, have been shown to be lower in density, biodegradable, inexpensive, and environmentally benign. Furthermore, the energy absorption capability and crashworthiness properties of composite tubes with diverse geometric shapes are highly dependent on the shape of the tubes. As a result of this research, circular cross-section tubes were shown to be an outstanding candidate in terms of energy absorption capability. Nonetheless, alternative forms of tubes, such as square, conical, and prism tubes, should be used in future study in order to achieve better results and to allow for better comparison. As for the trigger mechanism, suggested use variety type of trigger mechanism such as double chamfer trigger (DCT) tulip trigger (TT) and other type of trigger rather than just two type of trigger, it may lead the different result of each trigger use with different fibre orientation. In addition, dynamic loading tests should be included in experimental testing rather than just axial compression tests since they model actual crushing occurrences, which is more feasible in real world environments than.

REFERENCES

Abdullah, N., Sani, M., Salwani, M. and Husain, N., 2020. A review on crashworthiness studies of crash box structure. *Thin-Walled Structures*, 153, p.106795.

Albahash, Z. and Ansari, M., 2017. Investigation on energy absorption of natural and hybrid fiber under axial static crushing. *Composites Science and Technology*, 151, pp.52-61.

Asim, M., Jawaid, M., Saba, N., Nasir, M. and Sultan, M.T.H., 2017. Processing of hybrid polymer composites—a review. *Hybrid polymer composite materials*, pp.1-22.

Ataabadi, P., Karagiozova, D. and Alves, M., 2019. Crushing and energy absorption mechanisms of carbon fiber-epoxy tubes under axial impact. *International Journal of Impact Engineering*, 131, pp.174-189.

Batabyal, A., Nayak, R.K. and Tripathy, S., 2018. Evaluation of mechanical properties of glass fibre and carbon fibre reinforced polymer composite. *Journal of Communication Engineering & Systems*, *8*(2), pp.66-74.

Chambe, J., Bouvet, C., Dorival, O. and Ferrero, J., 2019. Energy absorption capacity of composite thin-wall circular tubes under axial crushing with different trigger initiations. *Journal of Composite Materials*, 54(10), pp.1281-1304.

Chandrasekar, M., Ishak, M.R., Jawaid, M., Sapuan, S.M. and Leman, Z., 2018. Low velocity impact properties of natural fiber-reinforced composite materials for aeronautical applications. In *Sustainable Composites for Aerospace Applications* (pp. 293-313). Woodhead Publishing.

Gupta, M.K., 2018. Investigations on Properties of Glass Fibre Reinforced Polymer Composite. *American Journal of Polymer Science & Engineering*, *6*(1), pp.31-44.

Işık, B. and Ekici, E., 2010. Experimental investigations of damage analysis in drilling of woven glass fiber-reinforced plastic composites. *The International Journal of Advanced Manufacturing Technology*, *49*(9), pp.861-869.

Khan, R., Mahdi, E. and Cabibihan, J., 2021. Effect of Fibre Orientation on the Quasi-Static Axial Crushing Behaviour of Glass Fibre Reinforced Polyvinyl Chloride Composite Tubes. *Materials*, 14(9), p.2235.

Kumar, Y. and Lohchab, D., 2016. Influence of Aviation Fuel on Mechanical properties of Glass Fiber-Reinforced Plastic Composite. *International Advanced Research Journal in Science, Engineering and Technology*, [online] 3(4), pp.58-66. Available at: <https://www.researchgate.net/publication/305996572_Influence_of_Aviation_Fuel_on_Mechanical_properties_of_Glass_Fiber-Reinforced_Plastic_Composite> [Accessed 2 February 2022].

Ma, Y., Sugahara, T., Yang, Y. and Hamada, H., 2015. A study on the energy absorption properties of carbon/aramid fiber filament winding composite tube. *Composite Structures*, 123, pp.301-311.

Mallick, P.K. ed., 1997. *Composites engineering handbook*. CRC Press.

Nasir Hussain, N., Regalla, S. and Daseswara Rao, Y., 2021. Study on influence of notch triggers on absorption of energy for composite automobile crash box under impact loads. *Materials Today: Proceedings*, 38, pp.3220-3231.

Pickering, K.L., Efendy, M.A. and Le, T.M., 2016. A review of recent developments in natural fibre composites and their mechanical performance. *Composites Part A: Applied Science and Manufacturing*, *83*, pp.98-112.

Raji, M., Abdellaoui, H., Essabir, H., Kakou, C., Bouhfid, R. and Qaiss, A., 2019. Prediction of the cyclic durability of woven-hybrid composites. *Durability and Life Prediction in Biocomposites, Fibre-Reinforced Composites and Hybrid Composites*, pp.27-62.

Saba, N. and Jawaid, M., 2017. Epoxy resin based hybrid polymer composites. In *Hybrid polymer composite materials* (pp. 57-82). Woodhead Publishing

Sathishkumar, T.P., Satheeshkumar, S. and Naveen, J., 2014. Glass fiber-reinforced polymer composites–a review. *Journal of reinforced plastics and composites*, *33*(13), pp.1258-1275.

Sivagurunathan, R., Lau Tze Way, S., Sivagurunathan, L. and Yaakob, M., 2018. The Effects of Triggering Mechanisms on the Energy Absorption Capability of Circular Jute/Epoxy Composite Tubes under Quasi-Static Axial Loading. *Applied Composite Materials*, 25(6), pp.1401-1417.

Sivagurunathan, R., Way, S., Sivagurunathan, L. and Yaakob, M., 2018. Effects of triggering mechanisms on the crashworthiness characteristics of square woven jute/epoxy composite tubes. *Journal of Reinforced Plastics and Composites*, 37(12), pp.824-840.

Supian, A., Sapuan, S., Zuhri, M., Zainudin, E., Ya, H. and Hisham, H., 2021. Effect of winding orientation on energy absorption and failure modes of filament wound kenaf/glass fibre reinforced epoxy hybrid composite tubes under intermediate-velocity impact (IVI) load. *Journal of Materials Research and Technology*, 10, pp.1-14.

Wambua, P., Ivens, J. and Verpoest, I., 2003. Natural fibres: can they replace glass in fibre reinforced plastics. *Composites science and technology*, *63*(9), pp.1259-1264.

Zhang, Z., Hou, S., Liu, Q. and Han, X., 2018. Winding orientation optimization design of composite tubes based on quasi-static and dynamic experiments. *Thin-Walled Structures*, 127, pp.425-433.

APPENDIX A1

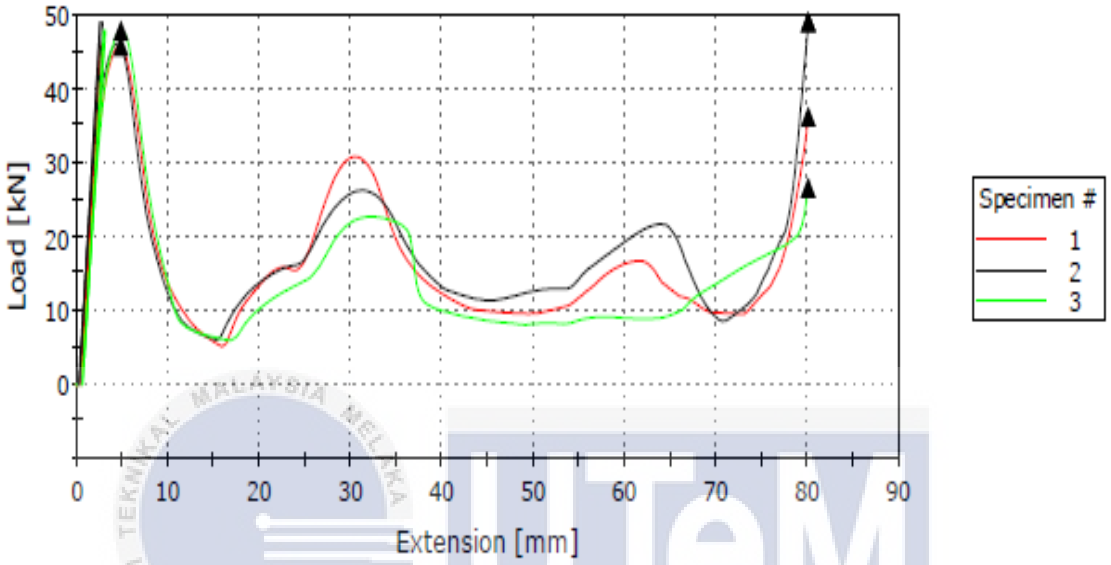

	Max Load [kN]	Compressive stress at Maximum Load [MPa]	Compressive strain (Extension) at Maximum Load [mm/mm]	Compressive extension at Maximum Load [mm]
1	> 45.686	> 39.198	> 0.050	> 4.90
2	> 48.936	> 41.986	> 0.816	> 80.01
3	> 47.788	> 41.001	> 0.050	> 4.87

	Modulus (E-modulus) [MPa]	Modulus (Automatic) [MPa]	Modulus (Automatic Young's) [MPa]
1	1500.932	1850.018	1845.236
2	1542.448	1816.100	1831.257
3	1543.844	1671.319	1781.003

Test result for ANC

APPENDIX A2

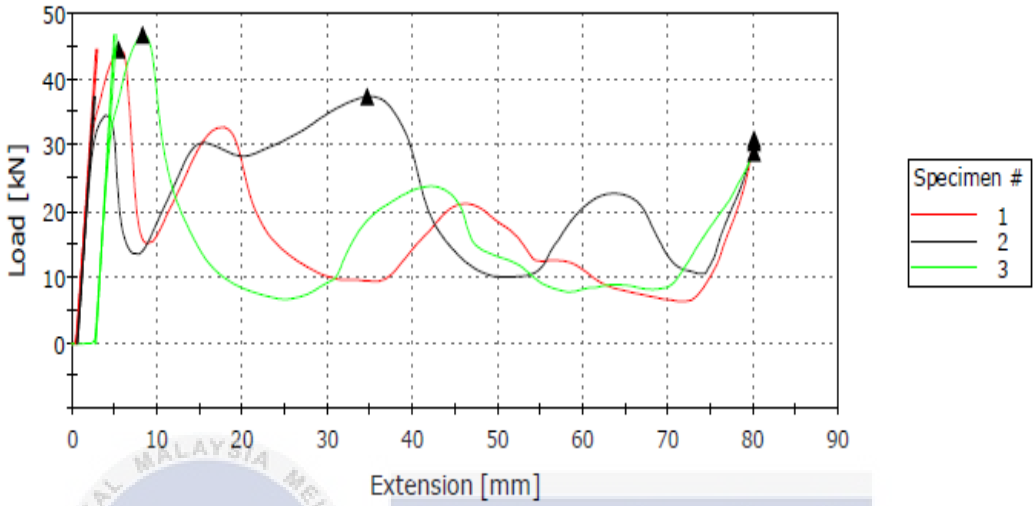

	Max Load [kN]	Compressive stress at Maximum Load [MPa]	Compressive strain (Extension) at Maximum Load [mm/mm]	Compressive extension at Maximum Load [mm]
1	> 44.443	> 38.131	> 0.056	> 5.48
2	> 37.312	> 32.013	> 0.354	> 34.65
3	> 46.660	> 40.033	> 0.085	> 8.33

	Modulus (E-modulus) [MPa]	Modulus (Automatic) [MPa]	Modulus (Automatic Young's) [MPa]
1	1450.688	1541.979	1640.156
2	1477.004	1571.528	1672.545
3	1540.224	1734.613	1830.018

Test result for ASC

APPENDIX A3

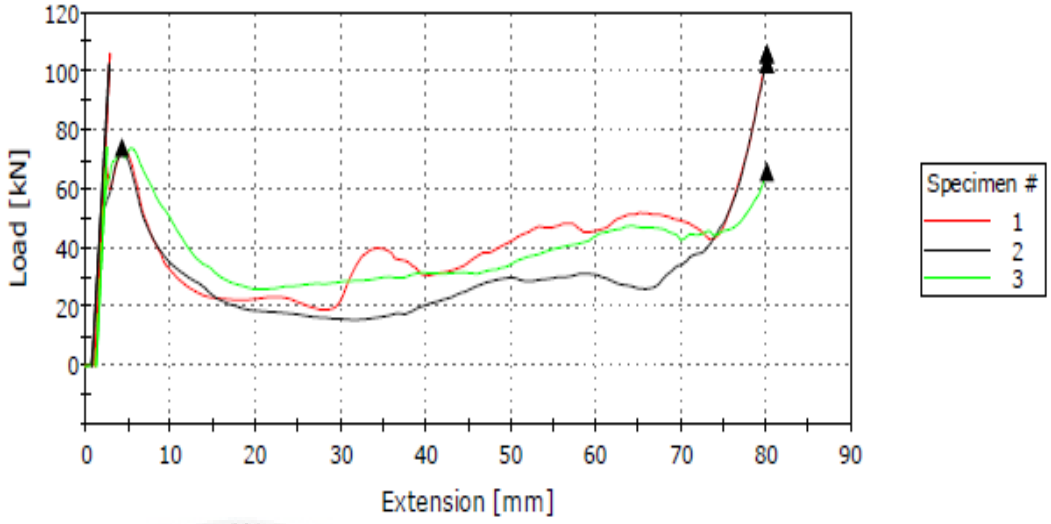

	Max Load [kN]	Compressive stress at Maximum Load [MPa]	Compressive strain (Extension) at Maximum Load [mm/mm]	Compressive extension at Maximum Load [mm]
1	> 106.006	> 90.950	> 0.816	> 80.02
2	> 102.407	> 87.863	> 0.816	> 80.02
3	> 74.063	> 63.545	> 0.044	> 4.27

	Modulus (E-modulus) [MPa]	Modulus (Automatic) [MPa]	Modulus (Automatic Young's) [MPa]
1	4995.015	5071.711	5174.632
2	4304.888	4010.668	4361.020
3	4875.695	4863.057	5104.535

Test result for BNC

APPENDIX A4

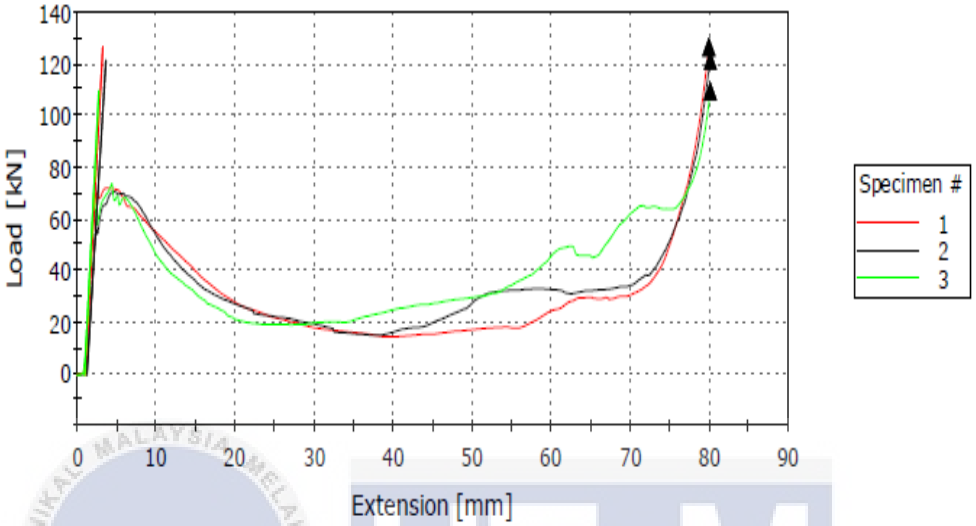

	Max Load [kN]	Compressive stress at Maximum Load [MPa]	Compressive strain (Extension) at Maximum Load [mm/mm]	Compressive extension at Maximum Load [mm]
1	> 126.353	> 108.408	> 0.814	> 79.82
2	> 121.151	> 103.945	> 0.816	> 80.01
3	> 109.417	> 93.877	> 0.816	> 80.01

	Modulus (E-modulus) [MPa]	Modulus (Automatic) [MPa]	Modulus (Automatic Young's) [MPa]
1	4683.228	4783.624	4800.487
2	4132.458	4295.021	4352.526
3	5085.786	5008.954	5183.709

Test result for BSC

APPENDIX A5

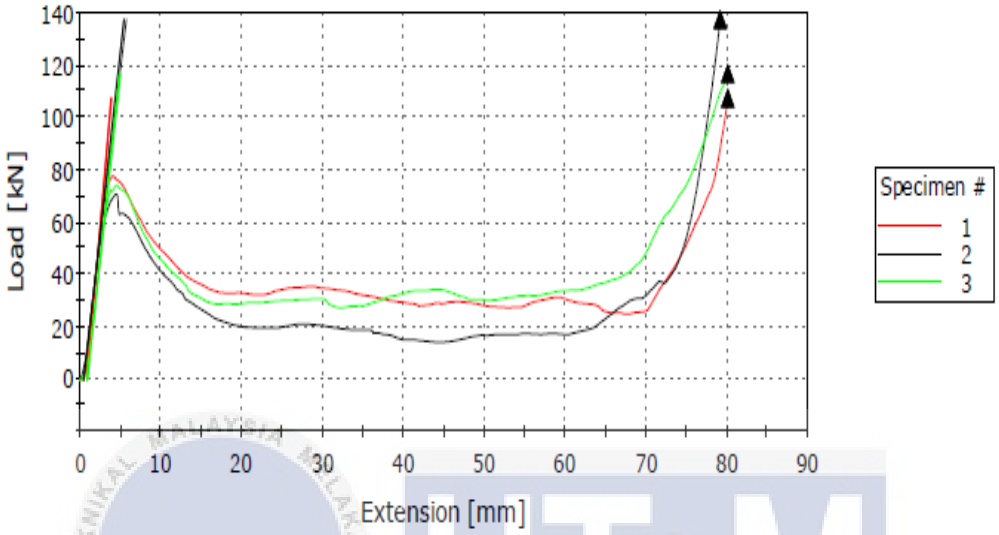

	Max Load [kN]	Compressive stress at Maximum Load [MPa]	Compressive strain (Extension) at Maximum Load [mm/mm]	Compressive extension at Maximum Load [mm]
1	> 107.252	> 92.020	> 0.816	> 80.01
2	> 137.145	> 74.880	> 0.807	> 79.07
3	> 116.639	> 70.051	> 0.816	> 80.01

	Modulus (E-modulus) [MPa]	Modulus (Automatic) [MPa]	Modulus (Automatic Young's) [MPa]
1	2894.817	3012.703	3034.812
2	1378.709	1485.384	1478.974
3	1641.735	1715.110	1737.919

Test result for CNC

APPENDIX A6

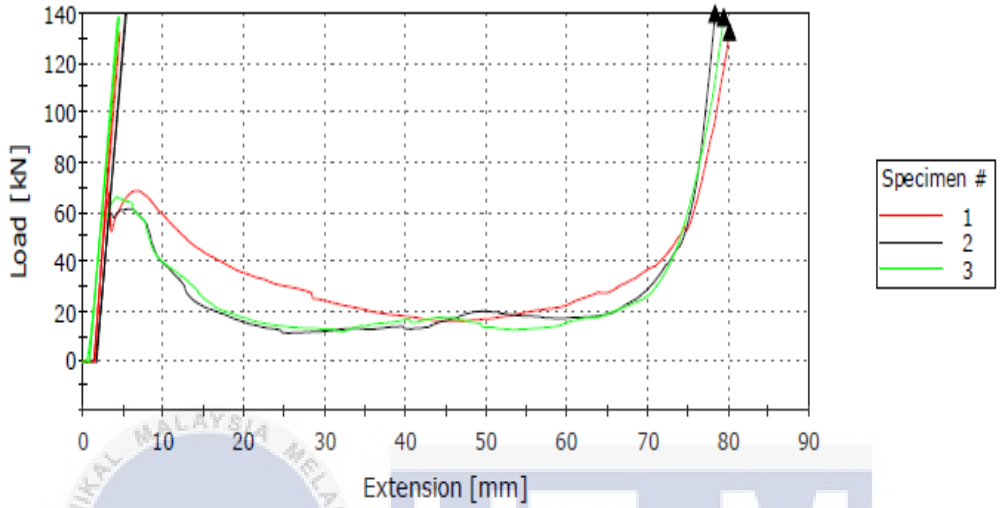

	Max Load [kN]	Compressive stress at Maximum Load [MPa]	Compressive strain (Extension) at Maximum Load [mm/mm]	Compressive extension at Maximum Load [mm]
1	> 132.269	> 72.217	> 0.816	> 80.01
2	> 139.623	> 119.793	> 0.798	> 78.24
3	> 138.108	> 118.494	> 0.809	> 79.28

	Modulus (E-modulus) [MPa]	Modulus (Automatic) [MPa]	Modulus (Automatic Young's) [MPa]
1	2198.170	2367.796	2556.329
2	3164.286	3180.662	3321.067
3	3075.104	3210.502	3360.293

Test result of CSC

APPENDIX A7

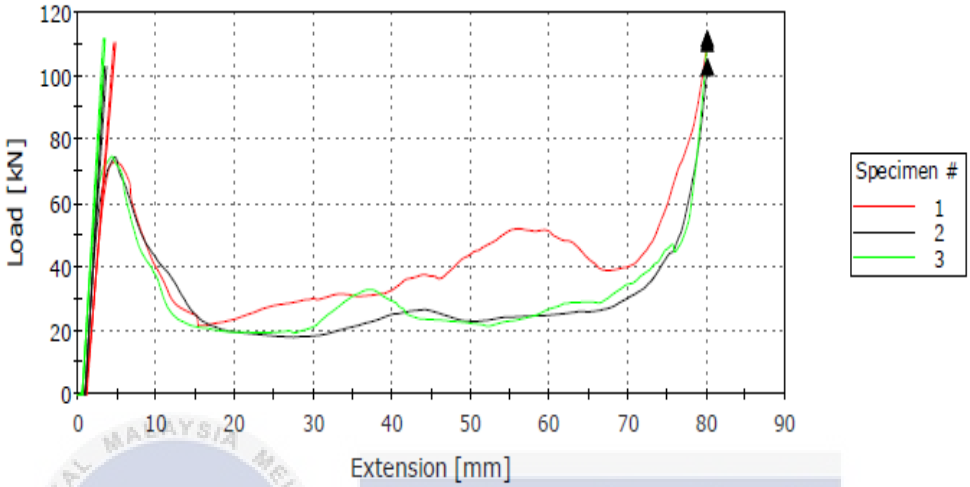

	Max Load [kN]	Compressive stress at Maximum Load [MPa]	Compressive strain (Extension) at Maximum Load [mm/mm]	Compressive extension at Maximum Load [mm]
1	> 110.169	> 94.523	> 0.816	> 80.01
2	> 102.656	> 88.076	> 0.816	> 80.01
3	> 111.453	> 95.624	> 0.816	> 80.01

	Modulus (E-modulus) [MPa]	Modulus (Automatic) [MPa]	Modulus (Automatic Young's) [MPa]
1	2497.334	2477.821	2699.678
2	3080.471	3519.591	3458.047
3	3191.551	3288.764	3597.410

Test result for DNC

APPENDIX A8

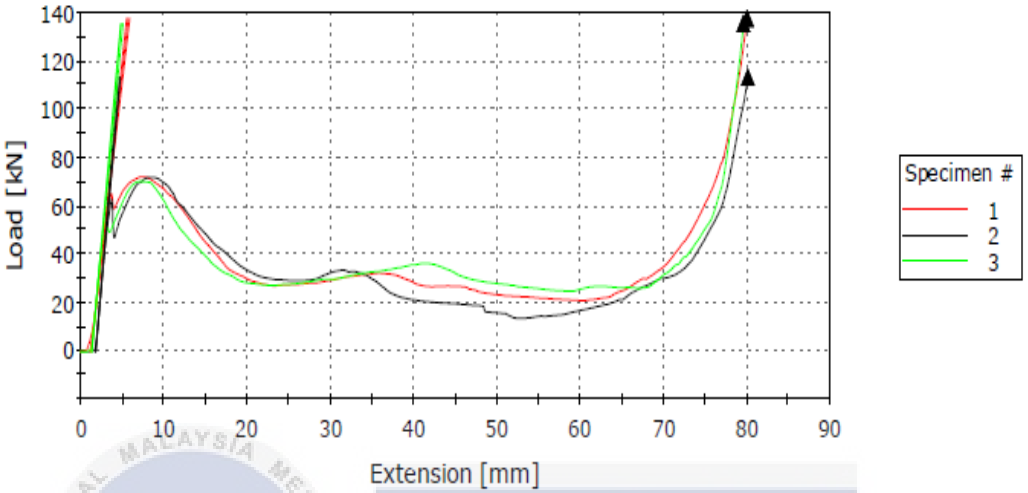

	Max Load [kN]	Compressive stress at Maximum Load [MPa]	Compressive strain (Extension) at Maximum Load [mm/mm]	Compressive extension at Maximum Load [mm]
1	> 137.269	> 117.774	> 0.815	> 79.91
2	> 113.064	> 97.007	> 0.816	> 80.01
3	> 135.125	> 115.934	> 0.811	> 79.50

	Modulus (E-modulus) [MPa]	Modulus (Automatic) [MPa]	Modulus (Automatic Young's) [MPa]
1	2575.335	2446.526	2734.301
2	3183.888	3278.741	3575.884
3	3238.222	3009.828	3310.225

Test result for DSC